

TENSOR-BASED METHODS FOR SEQUENTIAL STATE AND PARAMETER ESTIMATION IN STATE-SPACE MODELS

YIRAN ZHAO* AND TIANGANG CUI†

Abstract. Numerous real-world applications involve the filtering problem: one aims to sequentially estimate the states of a (stochastic) dynamical system from incomplete, indirect, and noisy observations over time to forecast and control the underlying system. Examples can be found in econometrics, meteorology, robotics, bioinformatics, and beyond. In addition to the filtering problem, it is often of interest to estimate some parameters that govern the evolution of the system. Both the filtering and the parameter estimation can be naturally formalized under the Bayesian framework. However, the Bayesian solution poses some significant challenges. For example, the most widely used particle filters can suffer from particle degeneracy and the more robust ensemble Kalman filters rely on the rather restrictive Gaussian assumptions. Exploiting the interplay between the low-rank tensor structure and Markov property of the filtering problem, we present a new approach for tackling Bayesian filtering and parameter estimation altogether. We also explore the preconditioning method to enhance the approximation power. Our approach aims at exact Bayesian solutions and does not suffer from particle degeneracy.

Key words. tensor train, state space model, sequential Monte Carlo, uncertainty quantification, Knothe–Rosenblatt rearrangement, transport maps

MSC codes. 68Q25, 68R10, 68U05

1. Introduction. State-space models have been widely used in mathematical and statistical modelling to understand time-varying complex phenomena [4, 16].

Examples include time series analysis in finance, temporal pattern recognition in bio-informatics, forecast in meteorology, etc. State-space models are also commonly referred to as hidden Markov models. A typical state-space model consists of two stochastic processes $\{\mathbf{X}_t\}_{t \geq 0}$ and $\{\mathbf{Y}_t\}_{t \geq 1}$. The state transition process $\{\mathbf{X}_t\}_{t \geq 0}$ is a \mathcal{X} -valued latent Markov process specified by a Markov transition density

$$(1.1) \quad \mathbf{X}_t | (\mathbf{X}_{0:t-1} = \mathbf{x}_{0:t-1}) \equiv \mathbf{X}_t | (\mathbf{X}_{t-1} = \mathbf{x}_{t-1}) \sim f(\mathbf{x}_t | \mathbf{x}_{t-1}, \boldsymbol{\theta})$$

and an initial density $p(\mathbf{x}_0 | \boldsymbol{\theta})$. Here \mathbf{X}_t represents the hidden state of the underlying system at an integer-valued time index $t \geq 0$ and the notation $\mathbf{x}_{i:j}$ denotes components $(\mathbf{x}_i, \mathbf{x}_{i+1}, \dots, \mathbf{x}_j)$ of a sequence $\{\mathbf{x}_t\}_{t \geq 0}$. The \mathcal{Y} -valued observation process $\{\mathbf{Y}_t\}_{t \geq 1}$ is characterized by the likelihood function $g(\mathbf{y}_t | \mathbf{x}_t, \boldsymbol{\theta})$ as

$$(1.2) \quad \mathbf{Y}_t | (\mathbf{X}_{0:t} = \mathbf{x}_{0:t}, \mathbf{Y}_{1:t-1} = \mathbf{y}_{1:t-1}) \equiv \mathbf{Y}_t | (\mathbf{X}_t = \mathbf{x}_t) \sim g(\mathbf{y}_t | \mathbf{x}_t, \boldsymbol{\theta}),$$

where \mathbf{Y}_t represents observables of the underlying system at time index $t > 0$. In (1.1) and (1.2), $\boldsymbol{\theta} \in \Theta$ is the set of parameters that govern the state transition and the observation.

Example 1.1. Volatility of financial derivatives. The stochastic volatility model consists of the logarithm of the volatility $\{\mathbf{X}_t\}_{t \geq 0}$ and the return of an asset $\{\mathbf{Y}_t\}_{t \geq 1}$. In the simplest setup, the log-volatility $\{\mathbf{X}_t\}_{t \geq 0}$ is a scalar-valued autoregressive process with order 1, i.e., $AR(1)$ process, while the scalar-valued return $\{\mathbf{Y}_t\}_{t \geq 1}$ is the observable determined by the volatility. The system is described as follows:

$$\begin{cases} \mathbf{X}_t &= \phi \mathbf{X}_{t-1} + \sigma \eta_t \\ \mathbf{Y}_t &= \epsilon_t \beta \exp(\mathbf{X}_t/2), \end{cases}$$

*School of Mathematics, Monash University, Victoria 3800, Australia yiran.zhao@monash.edu

†School of Mathematics, Monash University, Victoria 3800, Australia tiangang.cui@monash.edu

where $\Theta = (\phi, \sigma, \beta)$ are model parameters, ϵ_t and η_t are independent and identically distributed (i.i.d.) standard Gaussian random variables, and the initial state is given as $\mathbf{X}_0 \sim \mathcal{N}(0, \frac{\sigma^2}{1-\phi^2})$. The goal is to estimate the parameter Θ and the hidden states $\{\mathbf{X}_t\}_{t \geq 0}$ from observed return $\{\mathbf{Y}_t\}_{t \geq 1}$.

Following the state space model defined in (1.1) and (1.2), the joint probability density of $(\Theta, \mathbf{X}_{0:t}, \mathbf{Y}_{1:t})$ takes the form

$$(1.3) \quad p(\theta, \mathbf{x}_{0:t}, \mathbf{y}_{1:t}) = p(\theta) p(\mathbf{x}_0 | \theta) \prod_{j=1}^t f(\mathbf{x}_j | \mathbf{x}_{j-1}, \theta) \prod_{j=1}^k g(\mathbf{y}_j | \mathbf{x}_j, \theta),$$

where $p(\theta)$ and $p(\mathbf{x}_0 | \theta)$ are prescribed prior densities. Conditioned on all available data $\mathbf{Y}_{1:t} = \mathbf{y}_{1:t}$ at time t , the trajectory of the states $\mathbf{X}_{0:t}$ and the parameter Θ jointly follow the posterior density

$$(1.4) \quad p(\theta, \mathbf{x}_{0:t} | \mathbf{y}_{1:t}) = \frac{p(\theta, \mathbf{x}_{0:t}, \mathbf{y}_{1:t})}{p(\mathbf{y}_{1:t})},$$

where $p(\mathbf{y}_{1:t})$ is an unknown constant that is commonly referred to as the evidence. In this work, we aim to construct sequential algorithms that can simultaneously solve the following three inference problems at each time t :

- *Filtering*: Estimating the current state, which is the marginal conditional random variables

$$(1.5) \quad \mathbf{X}_t | (\mathbf{Y}_{1:t} = \mathbf{y}_{1:t}) \sim p(\mathbf{x}_t | \mathbf{y}_{1:t}) = \int p(\theta, \mathbf{x}_{0:t} | \mathbf{y}_{1:t}) d\mathbf{x}_{0:t-1} d\theta.$$

- *Parameter estimation*: Estimating the unknown parameter, which is the marginal conditional random variable

$$(1.6) \quad \Theta | (\mathbf{Y}_{1:t} = \mathbf{y}_{1:t}) \sim p(\theta | \mathbf{y}_{1:t}) = \int p(\theta, \mathbf{x}_{0:t} | \mathbf{y}_{1:t}) d\mathbf{x}_{0:t}.$$

- *Smoothing*: Estimating the trajectory of states, which are the marginal conditional random variables

$$(1.7) \quad \mathbf{X}_{0:t} | (\mathbf{Y}_{1:t} = \mathbf{y}_{1:t}) \sim p(\mathbf{x}_{0:t} | \mathbf{y}_{1:t}) = \int p(\theta, \mathbf{x}_{0:t} | \mathbf{y}_{1:t}) d\theta.$$

We want the algorithms to be *sequential* by design, i.e., the computation of new solutions to the problems defined in (1.5)–(1.7) at time t only relies on previous solutions at $t-1$ and the intermediate conditional densities in (1.1) and (1.2).

Estimation problems of these types have been extensively investigated in the literature. Assuming the parameter θ is known, the classical filtering problem aims to estimate the current state using $\mathbf{X}_t | (\mathbf{Y}_{1:t} = \mathbf{y}_{1:t}, \Theta = \theta)$ whereas the smoothing problem aims to estimate the trajectory of the states using $\mathbf{X}_{0:t} | (\mathbf{Y}_{1:t} = \mathbf{y}_{1:t}, \Theta = \theta)$. Various particle filter methods have been proposed to solve these two problems, see, e.g., [10, 23, 9, 19, 8]. The design principle of particle methods is to approximate the target distributions using a set of weighted particles and sequentially update the weights once new data are collected.

For systems with unknown parameters, the particle Markov chain Monte Carlo (MCMC) method [1] aims to estimate Θ from a batch of observed data $\mathbf{Y}_{1:t} = \mathbf{y}_{1:t}$. The particle MCMC method employs a Markov chain transition kernel invariant to the marginal posterior density $p(\theta | \mathbf{y}_{1:t})$ to solve the parameter estimation problem,

while the computationally intractable marginal posterior density $p(\boldsymbol{\theta}|\mathbf{y}_{1:t})$ is calculated using a particle filter over the state $\mathbf{X}_{0:t}$. This method can draw samples from the joint posterior $\boldsymbol{\Theta}, \mathbf{X}_{0:t} | (\mathbf{Y}_{1:t} = \mathbf{y}_{1:t})$, and thus can simultaneously solve the estimation problems in (1.5)–(1.7). However, the particle MCMC method can not update the inference in an online manner with new observed data.

To solve this problem, the SMC² method of [5] runs an outer-loop particle filter for updating the parameter distribution. Each of parameter samples is associated with an inner-loop particle filter of the states, which estimates the density $p(\boldsymbol{\theta}|\mathbf{y}_{1:t})$. Within SMC², a particle MCMC method is used as a restart step whenever the effective sample size of the parameter particles drops below some threshold. In general, particle methods are flexible to implement. But it comes at a potential cost that the weights, and hence the effective sample size, may degenerate with the number of time points and the state dimension [18, 22]. Moreover, the computational complexity for solving the sequential state and parameter estimation problems can be high. For example, the computational complexity of both the particle MCMC and the SMC² method increases linearly in the sample size of the parameters and quadratically in the time t .

In this paper, we present a set of new methods for solving the sequential state and parameter estimation problems. Instead of using particle-based method, the backbone of our methods is built upon the tensor-train decomposition [20, 21, 14, 12, 2], which is a scalable function approximation tool. We apply tensor trains to recursively approximate the time-varying joint posterior distributions. The separable form of tensor trains not only provides approximations to the marginal densities required in the three estimation problems mentioned above, but also naturally leads to a sequence of inverse Rosenblatt transports [25] that couple some reference random variables and the marginal random variables of interest. We then utilize these inverse Rosenblatt transports to remove the approximation bias using importance sampling and to precondition the tensor-train decomposition to further improve its approximation efficiency. Our method works well on several challenging numerical examples with linear computational complexity in the time, in contrast to the quadratic complexity of the SMC² method.

The rest of this paper is organized as follows. Section 2 introduces the background of the tensor-train decomposition and presents a basic implementation of the tensor-train-based algorithm. Section 3 presents an improved squared-tensor-train algorithm that is the key for deriving debiased sequential estimation methods using transport maps. Section 4 provides error analysis of the squared-tensor-train algorithm. Section 5 discusses preconditioning method for further improving the efficiency of tensor-train-based methods. Section 6 presents four numerical experiments to demonstrate the efficiency of our proposed methods and to compare with particle-based methods. Section 7 offers some concluding remarks.

2. Tensor train for recursive posterior approximation. In this section, we first introduce notation used throughout this paper. Then, we discuss the recursive formula that outlines the design principle of sequential estimation problems. Utilizing this recursive formula, we introduce tensor-train decomposition and present a basic implementation of the tensor-train-based sequential estimation algorithm.

2.1. Notation. The dimensionalities of the state space \mathcal{X} , the data space \mathcal{Y} , and the parameter space Θ are m , n , and d , respectively. We assume that the spaces \mathcal{X} , \mathcal{Y} , and Θ can be expressed as Cartesian products. We denote the j -th element of a vector \mathbf{x} by x_j . The index $t \in \mathbb{Z}$ is specifically reserved for denoting the time throughout the paper. This way, for a state random vector \mathbf{X}_t and its realization \mathbf{x}_t

at time t , their j -th elements are denoted by $X_{t,j}$ and $x_{t,j}$, respectively. Likewise, the same convention applies to the data vector \mathbf{Y}_t and its realization \mathbf{y}_t .

For a vector $\mathbf{x}_t \in \mathbb{R}^m$ and an index j , it is convenient to group a subset of elements using the following notation. The vector $\mathbf{x}_{t,<j} = [x_{t,1}, \dots, x_{t,j-1}]^\top$ collects the first $j-1$ elements, and the vector $\mathbf{x}_{t,>j} = [x_{t,j+1}, \dots, x_{t,m}]^\top$ collects the last $m-j$ elements. Similarly, we have $\mathbf{x}_{t,\leq j} = [x_{t,1}, \dots, x_{t,j}]^\top$, $\mathbf{x}_{t,\geq j} = [x_{t,j}, \dots, x_{t,m}]^\top$, and $\mathbf{x}_{t,\leq m} \equiv \mathbf{x}_{t,\geq 0} \equiv \mathbf{x}_t$.

We denote normalized posterior probability densities in the sequential estimation problems by p and its unnormalized version by π . Approximations to these densities are denoted by \tilde{p} and $\tilde{\pi}$, respectively. The notations \tilde{p} and $\tilde{\pi}$ are specifically reserved for their approximation in separable tensor-train format.

2.2. Recursive state and parameter estimation. Following the definition of the joint density of $(\Theta, \mathbf{X}_{0:t}, \mathbf{Y}_{1:t})$ in (1.3), the joint posterior density of $(\Theta, \mathbf{X}_{0:t})$ can also be expressed in a recursive form

$$(2.1) \quad p(\theta, \mathbf{x}_{0:t} | \mathbf{y}_{1:t}) = \frac{p(\theta, \mathbf{x}_{0:t-1} | \mathbf{y}_{1:t-1}) f(\mathbf{x}_t | \mathbf{x}_{t-1}, \theta) g(\mathbf{y}_t | \mathbf{x}_t, \theta)}{p(\mathbf{y}_t | \mathbf{y}_{1:t-1})},$$

where $p(\mathbf{y}_t | \mathbf{y}_{1:t-1})$ is some computationally intractable conditional evidence. Integrating both sides over $\mathbf{x}_{0:t-2}$, the parameter Θ and each pair of adjacent states $(\mathbf{X}_t, \mathbf{X}_{t-1})$ jointly follow the posterior density

$$(2.2) \quad p(\theta, \mathbf{x}_t, \mathbf{x}_{t-1} | \mathbf{y}_{1:t}) = \frac{p(\theta, \mathbf{x}_{t-1} | \mathbf{y}_{1:t-1}) f(\mathbf{x}_t | \mathbf{x}_{t-1}, \theta) g(\mathbf{y}_t | \mathbf{x}_t, \theta)}{p(\mathbf{y}_t | \mathbf{y}_{1:t-1})}.$$

The above formula outlines basic steps needed by a sequential estimation algorithm to solve the filtering problem (1.5) and the parameter estimation problem (1.6):

1. At time $t-1$, the existing posterior density for $(\Theta, \mathbf{X}_{t-1})$ is $p(\theta, \mathbf{x}_{t-1} | \mathbf{y}_{1:t-1})$.
2. At time t , using the state transition density $f(\mathbf{x}_t | \mathbf{x}_{t-1}, \theta)$ and the likelihood function $g(\mathbf{y}_t | \mathbf{x}_t, \theta)$ given by the observation process, we can compute the posterior density $p(\theta, \mathbf{x}_t, \mathbf{x}_{t-1} | \mathbf{y}_{1:t})$, up to the unknown evidence $p(\mathbf{y}_t | \mathbf{y}_{1:t-1})$.
3. Solving a marginalization problem

$$(2.3) \quad p(\theta, \mathbf{x}_t | \mathbf{y}_{1:t}) = \int_{\mathcal{X}} p(\theta, \mathbf{x}_t, \mathbf{x}_{t-1} | \mathbf{y}_{1:t}) d\mathbf{x}_{t-1},$$

we obtain the new posterior density $p(\theta, \mathbf{x}_t | \mathbf{y}_{1:t})$ for (Θ, \mathbf{X}_t) .

In these steps, the marginalization in (2.3) plays the key role in updating the joint posterior random variables (Θ, \mathbf{X}_t) . In the particle filter setting, one way to solve the marginalization is to draw conditional random variables $\mathbf{X}_t^{(i)} | \mathbf{X}_{t-1}^{(i)} = \mathbf{x}_{t-1}$ following conditional density $f(\mathbf{x}_t | \mathbf{x}_{t-1})$ for each of previous particles $\mathbf{X}_{t-1}^{(i)}$, and then update the weights using the likelihood function $g(\mathbf{y}_t | \mathbf{x}_t^{(i)})$, see the bootstrap filter [10] for details. The smoothing problem (1.7) can be solved by additional backpropagation steps given the solutions to the filtering and parameter estimation problems. In the rest of this section, we will introduce the tensor-train decomposition that can solve the marginalization problem (2.3) by function approximation, and then present a basic tensor-train-based algorithm to outline the procedure for solving the filtering and parameter estimation problems. Algorithms for solving the smoothing problem will be discussed in later sections.

2.3. Tensor-train decomposition. The central computational tool used in this work is the functional tensor-train decomposition [14, 12, 2]. Consider we have a

general multivariate function $f : \mathcal{X} \rightarrow \mathbb{R}$ where $\mathcal{X} \in \mathbb{R}^m$ is in the form of a Cartesian product. Then, one can approximately decompose $h(\mathbf{x})$ in the following form

$$h(\mathbf{x}) \approx \tilde{h}(\mathbf{x}) = \sum_{\alpha_0=1}^{r_0} \sum_{\alpha_1=1}^{r_1} \cdots \sum_{\alpha_m=1}^{r_m} \mathbf{H}_1^{(\alpha_0, \alpha_1)}(x_1) \cdots \mathbf{H}_k^{(\alpha_{k-1}, \alpha_k)}(x_k) \cdots \mathbf{H}_m^{(\alpha_{m-1}, \alpha_m)}(x_m),$$

where $r_0 = r_m = 1$ and the summation ranges r_0, r_1, \dots, r_m are called tensor-train ranks. Each scalar-valued univariate function $\mathbf{H}_k^{(\alpha_{k-1}, \alpha_k)}(x_k)$ is represented as a linear combination of a set of ℓ_k basis functions $\{\phi_k^{(1)}(x_k), \dots, \phi_k^{(\ell_k)}(x_k)\}$, which yields

$$\mathbf{H}_k^{(\alpha_{k-1}, \alpha_k)}(x_k) = \sum_{j=1}^{\ell_k} \phi_k^{(j)}(x_k) \mathbf{A}_k[\alpha_{k-1}, j, \alpha_k],$$

where $\mathbf{A}_k \in \mathbb{R}^{r_{k-1} \times \ell_k \times r_k}$ is an order-3 coefficient tensor. Examples of the basis functions include piecewise polynomials, orthogonal functions, radial basis functions, etc. Grouping all scalar-valued univariate functions $\mathbf{H}_k^{(\alpha_{k-1}, \alpha_k)}(x_k)$ for each coordinate x_k yields a matrix-valued function $\mathbf{H}_k(x_k) : \mathcal{X}_k \rightarrow \mathbb{R}^{r_{k-1} \times r_k}$, which is referred to as the k -th tensor core. This way, the decomposed function can also be expressed as a sequence of multiplications of matrix-valued univariate functions, which is given by

$$(2.4) \quad \tilde{h}(\mathbf{x}) = \mathbf{H}_1(x_1) \cdots \mathbf{H}_k(x_k) \cdots \mathbf{H}_m(x_m).$$

The tensor-train decomposition can be computed very efficiently without incurring the curse of dimensionality for a wide range of densities via alternating linear schemes together with cross approximation [20, 2, 11]. We employ the functional extension of the alternating minimal energy method with residual-based rank adaptation of [7]. It requires only $\mathcal{O}(mlr^2)$ evaluations of the function f and $\mathcal{O}(mlr^3)$ floating point operations, where $\ell = \max_k \ell_k$ and $r = \max_k r_k$. In general, the maximal rank r depends on the dimension m and can be large when the function f concentrates in some part of its domain. Some theoretical results exist that provide rank bounds. For example, the work of [24] establishes specific bounds for certain multivariate Gaussian densities that depend poly-logarithmically on m , while the work of [13] proves dimension-independent bounds for general functions in weighted spaces with dominating mixed smoothness.

Using the tensor-train decomposition, the integration of the factorized function can be simplified to integral of certain univariate tensor cores. For example, the integral over x_k can be calculated as

$$(2.5) \quad \begin{aligned} \int h(x_1, x_2, \dots, x_m) dx_k &\approx \int \mathbf{H}_1(x_k) \cdots \mathbf{H}_k(x_k) \cdots \mathbf{H}_m(x_m) dx_k \\ &= \mathbf{H}_1(x_1) \cdots \left(\int \mathbf{H}_k(x_k) dx_k \right) \cdots \mathbf{H}_m(x_m) \\ &= \mathbf{H}_1(x_1) \cdots \overline{\mathbf{H}}_k \cdots \mathbf{H}_m(x_m), \end{aligned}$$

where the overlined matrix $\overline{\mathbf{H}}_k \in \mathbb{R}^{r_{k-1} \times r_k}$ denotes the matrix after integrating the tensor core $\mathbf{H}_k(x_k)$. This way, the computational cost of the integration problem scales linearly in the dimensionality of variables and scales quadratically in the tensor-train ranks. This opens the door to solving the marginalization step in the sequential estimation problems discussed in Section 2.2.

2.4. Basic algorithm. Here we integrate the tensor-train decomposition and the recursive formula discussed in Section 2.2 to design a basic tensor-based algorithm for solving the sequential estimation problems.

At time $t - 1$, suppose the density of the posterior variables $\Theta, \mathbf{X}_{t-1} | (\mathbf{Y}_{1:t-1} = \mathbf{y}_{1:t-1})$ is approximated by a tensor train, i.e.,

$$p(\boldsymbol{\theta}, \mathbf{x}_{t-1} | \mathbf{y}_{1:t-1}) \propto \tilde{\pi}(\boldsymbol{\theta}, \mathbf{x}_{t-1} | \mathbf{y}_{1:t-1}),$$

where $a \propto b$ denotes that a is approximately proportional to b . Then, for new observed data \mathbf{y}_t , we can recursively approximate the new joint density of $\Theta, \mathbf{X}_t | (\mathbf{Y}_{1:t} = \mathbf{y}_{1:t})$, the filtering density of $\mathbf{X}_t | (\mathbf{Y}_{1:t} = \mathbf{y}_{1:t})$ and the parameter estimation density $\Theta | (\mathbf{Y}_{1:t} = \mathbf{y}_{1:t})$ as follows.

Algorithm 1: Sequential estimation using tensor trains.

(a) **Intermediate non-separable approximation.** Following (2.2), the joint posterior density of $\mathbf{X}_t, \Theta, \mathbf{X}_{t-1} | (\mathbf{Y}_{1:t} = \mathbf{y}_{1:t})$ yields an intermediate approximation

$$\begin{aligned} p(\mathbf{x}_t, \boldsymbol{\theta}, \mathbf{x}_{t-1} | \mathbf{y}_{1:t}) &\propto \hat{\pi}(\mathbf{x}_t, \boldsymbol{\theta}, \mathbf{x}_{t-1} | \mathbf{y}_{1:t}) \\ &= \tilde{\pi}(\mathbf{x}_{t-1}, \boldsymbol{\theta} | \mathbf{y}_{1:t-1}) f(\mathbf{x}_t | \mathbf{x}_{t-1}, \boldsymbol{\theta}) g(\mathbf{y}_t | \mathbf{x}_t, \boldsymbol{\theta}), \end{aligned}$$

where $\hat{\pi}$ is the unnormalized form that can be evaluated pointwise.

(b) **Separable approximation.** We approximate the intermediate unnormalized density $\hat{\pi}(\boldsymbol{\theta}, \mathbf{x}_t, \mathbf{x}_{t-1} | \mathbf{y}_{1:t})$ by a tensor-train decomposition

$$\begin{aligned} \hat{\pi}(\mathbf{x}_t, \boldsymbol{\theta}, \mathbf{x}_{t-1} | \mathbf{y}_{1:t}) &\approx \tilde{\pi}(\mathbf{x}_t, \boldsymbol{\theta}, \mathbf{x}_{t-1} | \mathbf{y}_{1:t}) \\ &= \mathbf{F}_1(x_{t,1}) \cdots \mathbf{F}_m(x_{t,m}) \mathbf{G}_1(\theta_1) \cdots \mathbf{G}_d(\theta_d) \mathbf{H}_1(x_{t-1,1}) \cdots \mathbf{H}_m(x_{t-1,m}), \end{aligned}$$

where \mathbf{F} , \mathbf{G} and \mathbf{H} denote tensor cores for the state at time t , the parameters, and the state at time $t - 1$, respectively.

(c) **Integration.** By integrating the approximation $\tilde{\pi}$, we are able to obtain the marginal posterior density for the joint random variable $\Theta, \mathbf{X}_t | (\mathbf{Y}_{1:t} = \mathbf{y}_{1:t})$

$$\begin{aligned} \tilde{\pi}(\mathbf{x}_t, \boldsymbol{\theta} | \mathbf{y}_{1:t}) &= \int \tilde{\pi}(\mathbf{x}_t, \boldsymbol{\theta}, \mathbf{x}_{t-1} | \mathbf{y}_{1:t}) d\mathbf{x}_{t-1} \\ &= \mathbf{F}_1(x_{t,1}) \cdots \mathbf{F}_m(x_{t,m}) \mathbf{G}_1(\theta_1) \cdots \mathbf{G}_d(\theta_d) (\bar{\mathbf{H}}_1 \cdots \bar{\mathbf{H}}_m), \end{aligned}$$

and the normalizing constant

$$c_t = \int \tilde{\pi}(\mathbf{x}_t, \boldsymbol{\theta}, \mathbf{x}_{t-1} | \mathbf{y}_{1:t}) d\mathbf{x}_t d\boldsymbol{\theta} d\mathbf{x}_{t-1} = \bar{\mathbf{F}}_1 \cdots \bar{\mathbf{F}}_m \bar{\mathbf{G}}_1 \cdots \bar{\mathbf{G}}_d \bar{\mathbf{H}}_1 \cdots \bar{\mathbf{H}}_m.$$

The posterior density for the parameter $\Theta | (\mathbf{Y}_{1:t} = \mathbf{y}_{1:t})$ and the posterior density for the state $\mathbf{X}_t | (\mathbf{Y}_{1:t} = \mathbf{y}_{1:t})$ can be obtained in a similar way.

In the next time step $t+1$, we can apply the same procedure using the newly computed approximation $\tilde{\pi}(\mathbf{x}_t, \boldsymbol{\theta} | \mathbf{y}_{1:t})$.

The above basic tensor-train-based algorithm reveals some of the key design principles of the algorithms introduced in this paper. Given the existing approximation, the joint density of $\Theta, \mathbf{X}_t, \mathbf{X}_{t-1} | (\mathbf{Y}_{1:t} = \mathbf{y}_{1:t})$ yields an intermediate approximation (step (a) of Alg. 1). Since the intermediate approximation does not have a separable

form, and hence cannot be marginalized, we reapproximate this intermediate approximation using a new tensor train (step (b) of Alg. 1) to carry all marginalization operations in the new iteration (step (c) of Alg. 1). We aim to design new algorithms that can remove estimation bias due to the approximation errors, as well as analyze the accumulation of approximation error over time. These will be discussed in Sections 3 and 4.

Moreover, the rank truncation used by the tensor-train may not preserve non-negativity of density functions. A two-dimensional analogue is that the truncated singular value decomposition of a non-negative matrix may contain negative entries. The non-negativity is essential for designing transport maps that are used for debiasing. We will overcome this barrier by introducing an alternative form of tensor-train decomposition. The computational complexity of the procedure presented here is quadratic in the tensor rank. Thus, we also develop preconditioning methods in Section 5 for reducing tensor ranks, in order to accelerate the computation.

3. Squared-tensor-train algorithms, debiasing and smoothing. In this section, we review the squared-tensor-train technique for building order-preserving transport maps, which is originally introduced in [6]. Then, we integrate the resulting transport maps into the recursive procedure defined in Section 2.4 to sequentially solve the filtering problem (1.5) and the parameter estimation problem (1.6) with sample-based debiasing. Based on this development, we also present an algorithm to solve the smoothing problem (1.7) with additional backpropagation steps.

3.1. Squared tensor train and Knothe–Rosenblatt rearrangement. Consider the normalized target probability density function $p(\mathbf{x}) = \frac{1}{z}\pi(\mathbf{x})$ with $\mathbf{x} \in \mathbb{R}^m$, in which z is an unknown constant and we can only evaluate the unnormalized density $\pi(\mathbf{x})$. To preserve non-negativity in function approximation, one can decompose the square root of $\pi(\mathbf{x})$, i.e.,

$$\sqrt{\pi(\mathbf{x})} \approx \phi(\mathbf{x}) = H_1(x_1) \cdots H_m(x_m).$$

Then, the approximate density function $\phi(\mathbf{x})^2$ is non-negative by construction. Given some reference probability density $\lambda(\mathbf{x}) := \prod_{i=1}^m \lambda_i(x_i)$ such that $\sup_{\mathbf{x}} \pi(\mathbf{x})/\lambda(\mathbf{x}) < \infty$, we can further construct a defensive version of the approximate density function

$$(3.1) \quad \tilde{p}(\mathbf{x}) = \frac{1}{\tilde{z}}\tilde{\pi}(\mathbf{x}), \quad \tilde{\pi}(\mathbf{x}) = \phi(\mathbf{x})^2 + \tau\lambda(\mathbf{x}), \quad \tilde{z} = \int \tilde{\pi}(\mathbf{x})d\mathbf{x},$$

for a sufficiently small constant $\tau > 0$. The approximate density $\tilde{p}(\mathbf{x})$ satisfies

$$\sup_{\mathbf{x}} \frac{p(\mathbf{x})}{\tilde{p}(\mathbf{x})} < \infty.$$

This bound is essential to ensure that importance sampling estimators defined by \tilde{p} can satisfy the central limit theorem. Based on some mild assumptions, the following lemma [6, Proposition 4, Theorem 1] establishes the error of the unnormalized approximation $\tilde{\pi}(\mathbf{x})$ and the normalized approximation $\tilde{p}(\mathbf{x})$.

LEMMA 3.1. *Suppose the error of the tensor-train approximation $\tilde{\pi}(\mathbf{x})$ satisfies $\|\phi - \sqrt{\pi}\|_{L^2} \leq \epsilon$ and the constant τ satisfies $\tau \leq \|\phi - \sqrt{\pi}\|_{L^2}^2$. Then, the L_2 distance between $\sqrt{\pi(\mathbf{x})}$ and $\sqrt{\tilde{\pi}(\mathbf{x})}$ defined in (3.1) satisfies $\|\sqrt{\pi(\mathbf{x})} - \sqrt{\tilde{\pi}(\mathbf{x})}\|_{L^2} \leq \sqrt{2\epsilon}$. Besides, the Hellinger distance between $p(\mathbf{x})$ and its normalized approximation $\tilde{p}(\mathbf{x})$ satisfies $D_H(p, \tilde{p}) \leq 2\epsilon/\sqrt{z}$.*

As outlined in Section 2.4, marginalization of the approximation is a key operation in deriving the recursive algorithm. For the squared tensor-train approximation defined in (3.1), the following proposition gives its marginal density.

PROPOSITION 3.2. *We consider the normalized approximation $\tilde{p}(\mathbf{x})$ defined in (3.1). For the tensor-train decomposition $\phi(\mathbf{x}) = \mathbf{H}_1(x_1) \cdots \mathbf{H}_m(x_m)$ and a given index $1 \leq k < m$, we define the left and right accumulated tensor cores as $\mathbf{H}_{\leq k}(\mathbf{x}_{\leq k}) = \mathbf{H}_1(x_1) \cdots \mathbf{H}_k(x_k) \in \mathbb{R}^{r_k}$ and $\mathbf{H}_{> k}(\mathbf{x}_{> k}) = \mathbf{H}_{k+1}(x_{k+1}) \cdots \mathbf{H}_m(x_m) \in \mathbb{R}^{r_k}$, respectively. Then the marginal density of $\tilde{p}(\mathbf{x})$ takes the form*

$$(3.2) \quad \tilde{p}(\mathbf{x}_{\leq k}) = \int \tilde{p}(\mathbf{x}) d\mathbf{x}_{> k} = \frac{1}{\tilde{z}} \left(\sum_{\gamma_k=1}^{r_k} \left(\sum_{\alpha_k=1}^{r_k} \mathbf{H}_{\leq k}^{(\alpha_k)}(\mathbf{x}_{\leq k}) \mathbf{L}_{> k}^{(\alpha_k, \gamma_k)} \right)^2 + \tau \lambda(\mathbf{x}_{\leq k}) \right),$$

where $\lambda(\mathbf{x}_{\leq k}) = \prod_{i=1}^k \lambda_i(x_i)$ and $\mathbf{L}_{> k} \in \mathbb{R}^{r_k \times r_k}$ is the (lower-triangular) Cholesky decomposition of the accumulated mass matrix

$$\mathbf{M}_{> k}^{(\alpha_k, \beta_k)} = \int \mathbf{H}_{> k}^{(\alpha_k)}(\mathbf{x}_{> k}) \mathbf{H}_{> k}^{(\beta_k)}(\mathbf{x}_{> k}) d\mathbf{x}_{> k}, \quad \alpha_k = 1, \dots, r_k, \quad \beta_k = 1, \dots, r_k.$$

Proof. The original proof is given in Proposition 2 of [6]. We illustrate the idea here for the sake of completeness. The marginal density $\tilde{p}(\mathbf{x}_{\leq k})$ is defined by integrating the approximation $\tilde{p}(\mathbf{x})$ over the coordinates in $\mathbf{x}_{> k}$, which takes the form

$$\begin{aligned} \int \tilde{p}(\mathbf{x}) d\mathbf{x}_{> k} &= \frac{1}{\tilde{z}} \left(\int \phi(\mathbf{x})^2 d\mathbf{x}_{> k} + \tau \int \lambda(\mathbf{x}) d\mathbf{x}_{> k} \right) \\ &= \frac{1}{\tilde{z}} \int \left(\sum_{\alpha_k=1}^{r_k} \mathbf{H}_{\leq k}^{(\alpha_k)}(\mathbf{x}_{\leq k}) \mathbf{H}_{> k}^{(\alpha_k)}(\mathbf{x}_{> k}) \right)^2 d\mathbf{x}_{> k} + \frac{\tau}{\tilde{z}} \lambda(\mathbf{x}_{\leq k}). \end{aligned}$$

The integral of the first term on the right hand side in the above equation can be expressed as

$$\begin{aligned} &\int \left(\sum_{\alpha_k=1}^{r_k} \mathbf{H}_{\leq k}^{(\alpha_k)}(\mathbf{x}_{\leq k}) \mathbf{H}_{> k}^{(\alpha_k)}(\mathbf{x}_{> k}) \right)^2 d\mathbf{x}_{> k} \\ &= \sum_{\alpha_k=1}^{r_k} \sum_{\beta_k=1}^{r_k} \mathbf{H}_{\leq k}^{(\alpha_k)}(\mathbf{x}_{\leq k}) \mathbf{H}_{\leq k}^{(\beta_k)}(\mathbf{x}_{\leq k}) \int \mathbf{H}_{> k}^{(\alpha_k)}(\mathbf{x}_{> k}) \mathbf{H}_{> k}^{(\beta_k)}(\mathbf{x}_{> k}) d\mathbf{x}_{> k} \\ &= \sum_{\alpha_k=1}^{r_k} \sum_{\beta_k=1}^{r_k} \mathbf{H}_{\leq k}^{(\alpha_k)}(\mathbf{x}_{\leq k}) \mathbf{H}_{\leq k}^{(\beta_k)}(\mathbf{x}_{\leq k}) \mathbf{M}_{> k}^{(\alpha_k, \beta_k)} \\ &= \sum_{\gamma_k=1}^{r_k} \left(\sum_{\alpha_k=1}^{r_k} \mathbf{H}_{\leq k}^{(\alpha_k)}(\mathbf{x}_{\leq k}) \mathbf{L}_{> k}^{(\alpha_k, \gamma_k)} \right)^2 \end{aligned}$$

where $\mathbf{L}_{> k} \mathbf{L}_{> k}^\top = \mathbf{M}_{> k}$. Then, the results follows. \square

As shown in [6, Section 3], the Cholesky decomposition in Proposition 3.2 can be recursively computed from $k = m - 1$ to $k = 1$. The normalizing constant \tilde{z} can also be computed in a similar way as the last iteration of the recursion. Computing all marginal densities $\tilde{p}(x_1), \dots, \tilde{p}(x_{m-1})$ requires $\mathcal{O}(mlr^3)$ floating point operations.

Using the marginal densities constructed in Proposition 3.2, the densities of the sequence of random variables $X_1, X_2 | X_1, \dots, X_k | \mathbf{X}_{< k}, \dots$ can be approximated by $\tilde{p}(x_1)$ and

$$\tilde{p}(x_k | \mathbf{x}_{< k}) = \frac{\tilde{p}(\mathbf{x}_{\leq k})}{\tilde{p}(\mathbf{x}_{< k})} = \frac{\phi(\mathbf{x}_{\leq k})^2 + \tau \lambda(\mathbf{x}_{\leq k})}{\phi(\mathbf{x}_{< k})^2 + \tau \lambda(\mathbf{x}_{< k})},$$

respectively. The corresponding approximate distribution functions

$$(3.3) \quad F_1(x_1) = \int_{-\infty}^{x_1} \tilde{p}(x'_1) dx'_1 \quad \text{and} \quad F_k(x_k | \mathbf{x}_{<k}) = \int_{-\infty}^{x_k} \tilde{p}(x'_k | \mathbf{x}_{<k}) dx'_k$$

defines an order-preserving map $\mathcal{F} : \mathbb{R}^m \mapsto [0, 1]^m$ in the form of

$$(3.4) \quad \mathcal{F}(\mathbf{x}) = [F_1(x_1), \dots, F_k(x_k | \mathbf{x}_{<k}), \dots, F_m(x_m | \mathbf{x}_{<m})]^\top,$$

which is commonly referred to as the Knothe–Rosenblatt (KR) rearrangement [25, 17]. The map \mathcal{F} transforms a random variable $\mathbf{X} \sim \tilde{p}(\mathbf{x})$ into a uniform random variable in the hypercube $[0, 1]^m$, i.e., $\mathbf{U} = \mathcal{F}(\mathbf{X})$ with $\mathbf{U} \sim \text{Uni}(\mathbf{u}; [0, 1]^m)$. Since the k -th component of the map \mathcal{F} depends on only the previous $k - 1$ coordinates, both the map \mathcal{F} and its inverse have triangular structures, and thus can be evaluated dimension-by-dimension.

The computational complexity of evaluating \mathcal{F} is dominated by the dimension-by-dimension evaluation of the conditional densities $\tilde{p}(x_k | \mathbf{x}_{<k})$, $k = 2, \dots, m$ and the corresponding distribution functions, which is $\mathcal{O}(m\ell r^2)$ in total. Compared to the computational complexity of constructing all marginal densities, evaluating the above defined KR rearrangement is less costly.

Remark 3.3. Note the marginal density $\tilde{p}(\mathbf{x}_{\geq k})$, $k = 2, \dots, m$ can be approximated in a similar way from the first coordinate to the last coordinate. In this way, the resulting KR rearrangement is upper-triangular, i.e.,

$$(3.5) \quad \mathcal{F}^u(\mathbf{x}) = [F_1(x_1 | \mathbf{x}_{>1}), \dots, F_k(x_k | \mathbf{x}_{>k}), \dots, F_m(x_m)]^\top,$$

as the variable dependency follows a reverse order.

3.2. Non-negativity-preserving algorithm and auxiliary particle filter.

Following the steps of the basic algorithm (cf. Alg. 1), we first define a new sequential estimation algorithm using the non-negativity-preserving approximation presented in (3.1). Then, we utilize the associated KR rearrangement to sequentially generate weighted samples to correct for approximation bias.

Algorithm 2: Sequential estimation using squared-tensor-train approximations.

- (a) **Intermediate non-separable approximation.** At time $t - 1$, suppose the joint posterior density $p(\boldsymbol{\theta}, \mathbf{x}_{t-1} | \mathbf{y}_{1:t-1})$ is approximated by an unnormalized density $\tilde{\pi}(\boldsymbol{\theta}, \mathbf{x}_{t-1} | \mathbf{y}_{1:t-1})$. The density of $\mathbf{X}_t, \boldsymbol{\theta}, \mathbf{X}_{t-1} | (\mathbf{Y}_{1:t} = \mathbf{y}_{1:t})$ yields an intermediate approximation

$$(3.6) \quad p(\mathbf{x}_t, \boldsymbol{\theta}, \mathbf{x}_{t-1} | \mathbf{y}_{1:t}) \propto \hat{\pi}(\mathbf{x}_t, \boldsymbol{\theta}, \mathbf{x}_{t-1} | \mathbf{y}_{1:t}) \\ = \tilde{\pi}(\mathbf{x}_{t-1}, \boldsymbol{\theta} | \mathbf{y}_{1:t-1}) f(\mathbf{x}_t | \mathbf{x}_{t-1}, \boldsymbol{\theta}) g(\mathbf{y}_t | \mathbf{x}_t, \boldsymbol{\theta}).$$

- (b) **Separable approximation.** We approximate the square root of $\hat{\pi}$ by a tensor-train decomposition

$$(3.7) \quad \sqrt{\hat{\pi}(\mathbf{x}_t, \boldsymbol{\theta}, \mathbf{x}_{t-1} | \mathbf{y}_{1:t})} \\ \approx \phi_t(\mathbf{x}_t, \boldsymbol{\theta}, \mathbf{x}_{t-1}) \\ = \mathbf{G}_1(x_{t,1}) \cdots \mathbf{G}_m(x_{t,m}) \mathbf{F}_1(\theta_1) \cdots \mathbf{F}_d(\theta_d) \mathbf{H}_1(x_{t-1,1}) \cdots \mathbf{H}_m(x_{t-1,m}).$$

and choose a constant τ such that $\tau \leq \|\phi_t - \sqrt{\hat{\pi}}\|_{L^2}^2$. This gives an approximation to $\hat{\pi}(\mathbf{x}_t, \boldsymbol{\theta}, \mathbf{x}_{t-1} | \mathbf{y}_{1:t})$ in the form of

$$(3.8) \quad \hat{\pi}(\mathbf{x}_t, \boldsymbol{\theta}, \mathbf{x}_{t-1} | \mathbf{y}_{1:t}) = \phi_t(\mathbf{x}_t, \boldsymbol{\theta}, \mathbf{x}_{t-1})^2 + \tau \lambda(\mathbf{x}_t) \lambda(\boldsymbol{\theta}) \lambda(\mathbf{x}_{t-1}).$$

(c) **Integration.** We apply Proposition 3.2 from right to left to obtain $\tilde{\pi}(\mathbf{x}_t, \boldsymbol{\theta} | \mathbf{y}_{1:t}) = \int \tilde{\pi}(\mathbf{x}_t, \boldsymbol{\theta}, \mathbf{x}_{t-1} | \mathbf{y}_{1:t}) d\mathbf{x}_{t-1}$ and $\tilde{z}_t = \int \tilde{\pi}(\mathbf{x}_t, \boldsymbol{\theta}, \mathbf{x}_{t-1} | \mathbf{y}_{1:t}) d\mathbf{x}_t d\boldsymbol{\theta} d\mathbf{x}_{t-1}$.

In the next time step $t+1$, we can apply the same procedure using the newly computed marginal approximation $\tilde{\pi}(\mathbf{x}_t, \boldsymbol{\theta} | \mathbf{y}_{1:t})$.

In step (b) of Alg. 2, the approximation $\tilde{\pi}(\mathbf{x}_t, \boldsymbol{\theta}, \mathbf{x}_{t-1} | \mathbf{y}_{1:t})$ is guaranteed to be non-negative. The approximation $\tilde{\pi}$ defines a normalized approximate density of the posterior random variables $\mathbf{X}_t, \boldsymbol{\Theta}, \mathbf{X}_{t-1} | (\mathbf{Y}_{1:t} = \mathbf{y}_{1:t})$ in the form of

$$\tilde{p}(\mathbf{x}_t, \boldsymbol{\theta}, \mathbf{x}_{t-1} | \mathbf{y}_{1:t}) = \frac{1}{\tilde{z}_t} \tilde{\pi}(\mathbf{x}_t, \boldsymbol{\theta}, \mathbf{x}_{t-1} | \mathbf{y}_{1:t}),$$

where \tilde{z}_t is obtained in step (c) of Alg. 2. One can apply Proposition 3.2 to integrate the approximate density $\tilde{\pi}$ from left (the variable $x_{t,1}$) to right (the variable $x_{t-1,m}$) to define an upper-triangular KR rearrangement $\mathcal{F}_t^u : \mathcal{X} \times \Theta \times \mathcal{X} \rightarrow [0, 1]^{2m+d}$ in the form of

$$(3.9) \quad \mathcal{F}_t^u(\mathbf{x}_t, \boldsymbol{\theta}, \mathbf{x}_{t-1}) = \begin{bmatrix} \mathcal{F}_t^u(\mathbf{x}_t | \boldsymbol{\theta}, \mathbf{x}_{t-1}) \\ \mathcal{F}_t^u(\boldsymbol{\theta} | \mathbf{x}_{t-1}) \\ \mathcal{F}_t^u(\mathbf{x}_{t-1}) \end{bmatrix} = \begin{bmatrix} F_{t,1} & (x_{t,1} & | \mathbf{x}_{t,>1}, \boldsymbol{\theta}, \mathbf{x}_{t-1}) \\ \vdots & \vdots & \vdots \\ F_{t,m} & (x_{t,m} & | \boldsymbol{\theta}, \mathbf{x}_{t-1}) \\ \vdots & \vdots & \vdots \\ F_{\theta,k} & (\theta_k & | \boldsymbol{\theta}_{>k}, \mathbf{x}_{t-1}) \\ \vdots & \vdots & \vdots \\ F_{t-1,1} & (x_{t-1,1} & | \mathbf{x}_{t-1,>1}) \\ \vdots & \vdots & \vdots \\ F_{t-1,m} & (x_{t-1,m}) \end{bmatrix},$$

where the middle term is the KR rearrangement in a block-upper-triangular form. The following proposition paves the way for removing approximation bias by generating weighted samples using the map \mathcal{F}_t^u .

PROPOSITION 3.4. *Suppose we have samples $\{\boldsymbol{\Theta}^{(i)}, \mathbf{X}_{0:t-1}^{(i)}, W_{t-1}^{(i)}\}_{i=1}^N$ that follow the joint density $p(\boldsymbol{\theta}, \mathbf{x}_{0:t-1} | \mathbf{y}_{1:t-1})$ at time $t-1$. Then conditioned on each pair of $\{\boldsymbol{\Theta}^{(i)}, \mathbf{X}_{t-1}^{(i)}\}_{i=1}^N$, we can invert the first block of \mathcal{F}_t^u in (3.9) to obtain a new sample*

$$(3.10) \quad \mathbf{X}_t^{(i)} = (\mathcal{F}_t^u)^{-1}(\mathbf{U} | \boldsymbol{\Theta}^{(i)}, \mathbf{X}_{t-1}^{(i)}), \quad \mathbf{U} \sim \text{Uni}(\mathbf{u}; [0, 1]^m).$$

The sample $\mathbf{X}_t^{(i)}$ follows the conditional density $\tilde{p}(\mathbf{x}_t | \boldsymbol{\theta}, \mathbf{x}_{t-1}, \mathbf{y}_{1:t})$. Expanding the sample state path $\mathbf{X}_{0:t-1}^{(i)}$ by $\mathbf{X}_t^{(i)}$, the updated weighted samples $\{\boldsymbol{\Theta}^{(i)}, \mathbf{X}_{0:t}^{(i)}, W_{t-1}^{(i)}\}_{i=1}^N$ jointly follow the normalized density $\tilde{p}(\mathbf{x}_t | \boldsymbol{\theta}, \mathbf{x}_{t-1}, \mathbf{y}_{1:t}) p(\boldsymbol{\theta}, \mathbf{x}_{0:t-1} | \mathbf{y}_{1:t-1})$.

Proof. Conditioned on $\boldsymbol{\Theta}^{(i)} = \boldsymbol{\theta}, \mathbf{X}_{t-1}^{(i)} = \mathbf{x}_{t-1}$, the Jacobian of $\mathcal{F}_t^u(\cdot | \boldsymbol{\theta}, \mathbf{x}_{t-1})$, denoted by $\mathbf{J} \in \mathbb{R}^{m \times m}$, is an upper triangular matrix with diagonal entries

$$J_{kk} = \frac{\partial F_{t,k}(x_{t,k} | \mathbf{x}_{t,>k}, \boldsymbol{\theta}, \mathbf{x}_{t-1})}{\partial x_{t,k}} = \tilde{p}(x_{t,k} | \mathbf{x}_{t,>k}, \boldsymbol{\theta}, \mathbf{x}_{t-1}, \mathbf{y}_{1:t}), \quad k = 1, \dots, m.$$

Thus, the pullback of the uniform density $\text{Uni}(\mathbf{u}; [0, 1]^m)$ under $\mathcal{F}_t^u(\cdot | \boldsymbol{\theta}, \mathbf{x}_{t-1})$ is

$$|\mathbf{J}| = \prod_{k=1}^m \tilde{p}(x_{t,k} | \mathbf{x}_{t,>k}, \boldsymbol{\theta}, \mathbf{x}_{t-1}, \mathbf{y}_{1:t}) = \tilde{p}(\mathbf{x}_t | \boldsymbol{\theta}, \mathbf{x}_{t-1}, \mathbf{y}_{1:t}).$$

Hence, the conditional sample $\mathbf{X}_t^{(i)} | \boldsymbol{\Theta}^{(i)}, \mathbf{X}_{t-1}^{(i)}$ has the density $\tilde{p}(\mathbf{x}_t | \boldsymbol{\Theta}^{(i)}, \mathbf{X}_{t-1}^{(i)}, \mathbf{y}_{1:t})$. The rest of the result directly follows. \square

After applying the sampling procedure in (3.10), we can update the weights of the updated samples $\{\Theta^{(i)}, \mathbf{X}_{0:t}^{(i)}, W_{t-1}^{(i)}\}_{i=1}^N$ according to the new joint posterior density $p(\boldsymbol{\theta}, \mathbf{x}_{0:t} | \mathbf{y}_{1:t})$. Following the recursive form of the density $p(\boldsymbol{\theta}, \mathbf{x}_{0:t} | \mathbf{y}_{1:t})$ in (2.1), the importance weights can be updated by the function

$$(3.11) \quad \omega(\boldsymbol{\theta}, \mathbf{x}_{t-1:t}) = \frac{p(\boldsymbol{\theta}, \mathbf{x}_{0:t} | \mathbf{y}_{1:t})}{\tilde{p}(\mathbf{x}_t | \boldsymbol{\theta}, \mathbf{x}_{t-1}, \mathbf{y}_{1:t}) p(\boldsymbol{\theta}, \mathbf{x}_{0:t-1} | \mathbf{y}_{1:t-1})} = \frac{f(\mathbf{x}_t | \mathbf{x}_{t-1}, \boldsymbol{\theta}) g(\mathbf{y}_t | \mathbf{x}_t, \boldsymbol{\theta})}{\tilde{p}(\mathbf{x}_t | \boldsymbol{\theta}, \mathbf{x}_{t-1}, \mathbf{y}_{1:t})}.$$

Algorithm 3 provides details of the particle filter accompanying the sequential estimation procedure in Alg. 2.

Algorithm 3: One iteration of the particle filter accompanying Alg. 2.

- (a) At time $t-1$, suppose we have weighted samples $\{\Theta^{(i)}, \mathbf{X}_{0:t-1}^{(i)}, W_{t-1}^{(i)}\}_{i=1}^N$ following the joint density $p(\boldsymbol{\theta}, \mathbf{x}_{0:t-1} | \mathbf{y}_{1:t-1})$.
 - (b) At time t , given the approximate density $\tilde{\pi}(\mathbf{x}_t, \boldsymbol{\theta}, \mathbf{x}_{t-1} | \mathbf{y}_{1:t})$ computed in step (b) of Alg. 2, apply Proposition 3.2 to integrate the approximate density $\tilde{\pi}$ from left to right to define a KR rearrangement \mathcal{F}_t^u in the form of (3.9).
 - (c) For each of $\{\Theta^{(i)}, \mathbf{X}_{0:t-1}^{(i)}\}_{i=1}^N$, invert the first block of \mathcal{F}_t^u as in (3.10) to generate a new sample $\mathbf{X}_t^{(i)}$, and then update the weights according to $W_t^{(i)} = W_{t-1}^{(i)} \omega(\Theta^{(i)}, \mathbf{X}_{t-1:t}^{(i)})$, where the function $\omega(\cdot, \cdot)$ is defined in (3.11).
 - (d) Renormalize the weights $W_t^{(i)} \leftarrow W_t^{(i)} / \sum_{i=1}^N W_t^{(i)}$.
-

Algorithm 3 can be viewed as an auxiliary particle filter [22] as it uses the next observation to construct the proposal density. Commonly used resampling techniques in sequential Monte Carlo methods can also be used in Alg. 3 as a rejuvenation step to re-balance the weights.

3.3. Particle smoothing. Similar to other particle filter algorithms, weights computed by Algorithm 3 may degenerate over time. This has an intuitive explanation in the joint parameter estimation context. The locations of the parameter samples are fixed at the initial time, so that the weights (and hence the effective sample size) necessarily degenerate because the parameter posterior may concentrate with more data observed over time. One way to overcome this issue is to apply particle smoothing instead of the reweighting of Alg. 3.

Particle smoothing uses the same sequence of non-negative-preserving approximations constructed in Alg. 2. At each time step $1 \leq t \leq T$, we can integrate the approximate density $\tilde{\pi}(\mathbf{x}_t, \boldsymbol{\theta}, \mathbf{x}_{t-1} | \mathbf{y}_{1:t})$ from right (the variable $x_{t-1,m}$) to left (the variable $x_{t,1}$) to define the corresponding lower-triangular KR rearrangement

$$(3.12) \quad \mathcal{F}_t^l(\mathbf{x}_t, \boldsymbol{\theta}, \mathbf{x}_{t-1}) = \begin{bmatrix} \mathcal{F}_t^l(\mathbf{x}_t) \\ \mathcal{F}_t^l(\boldsymbol{\theta} \mid \mathbf{x}_t) \\ \mathcal{F}_t^l(\mathbf{x}_{t-1} | \boldsymbol{\theta}, \mathbf{x}_t) \end{bmatrix} = \begin{bmatrix} F_{t,1} & (x_{t,1}) \\ & \vdots \\ F_{t,m} & (x_{t,m} \mid \mathbf{x}_{t,<m}) \\ & \vdots \\ F_{\theta,k} & (\theta_k \mid \mathbf{x}_{t,<k}) \\ & \vdots \\ F_{t-1,1} & (x_{t-1,1} \mid \mathbf{x}_t, \boldsymbol{\theta}) \\ & \vdots \\ F_{t-1,m} & (x_{t-1,m} \mid \mathbf{x}_t, \boldsymbol{\theta}, \mathbf{x}_{t-1,<m}) \end{bmatrix}.$$

In the following proposition, we use the sequence of KR rearrangements $\{\mathcal{F}_t^l\}_{t=1}^T$ to define a backward sampling procedure, starting at time T , and the corresponding sampling density.

PROPOSITION 3.5. Consider KR rearrangements $\{\mathcal{F}_t^l\}_{t=1}^T$ defined in (3.12). At time T , samples $\{\mathbf{X}_{T-1}^{(i)}, \mathbf{X}_T^{(i)}, \Theta^{(i)}\}_{i=1}^N$ are generated from $\tilde{p}(\mathbf{x}_T, \boldsymbol{\theta}, \mathbf{X}_{t-1} | \mathbf{y}_{1:T})$ using \mathcal{F}_T^l . Then, at each of steps $t = T-1, \dots, 1$, for each of $\{\Theta^{(i)}, \mathbf{X}_{t:T}^{(i)}\}_{i=1}^N$, invert the last block of the KR rearrangements $\mathcal{F}_t^l(\cdot | \boldsymbol{\theta}, \mathbf{x}_t)$ to obtain

$$(3.13) \quad \mathbf{X}_{t-1}^{(i)} = (\mathcal{F}_t^l)^{-1}(\mathbf{U} | \Theta^{(i)}, \mathbf{X}_t^{(i)}), \quad \mathbf{U} \sim \text{Uni}(\mathbf{u}; [0, 1]^m).$$

After completing backward recursion, each pair of the parameter sample and state path sample in $\{\Theta^{(i)}, \mathbf{X}_{0:T}^{(i)}\}_{i=1}^N$ follows the joint density

$$\tilde{p}(\boldsymbol{\theta}, \mathbf{x}_{0:T} | \mathbf{y}_{1:T}) = \tilde{p}(\mathbf{x}_T, \boldsymbol{\theta}, \mathbf{x}_{T-1} | \mathbf{y}_{1:T}) \prod_{t=1}^{T-1} \tilde{p}(\mathbf{x}_{t-1} | \boldsymbol{\theta}, \mathbf{x}_t, \mathbf{y}_{1:t}).$$

Proof. The proof follows a similar reasoning as that of Proposition 3.4. We omit the details for brevity. \square

For a pair of sample parameter and sample state path $(\Theta^{(i)} = \boldsymbol{\theta}, \mathbf{X}_{0:T}^{(i)} = \mathbf{x}_{0:T})$ generated as in Proposition 3.5, it yields a weight representation of the posterior sample with the importance weight

$$(3.14) \quad \begin{aligned} \omega(\boldsymbol{\theta}, \mathbf{x}_{0:T}) &= \frac{p(\boldsymbol{\theta}, \mathbf{x}_{0:T} | \mathbf{y}_{1:T})}{\tilde{p}(\boldsymbol{\theta}, \mathbf{x}_{0:T} | \mathbf{y}_{1:T})} \\ &\propto p(\boldsymbol{\theta}) p(\mathbf{x}_0 | \boldsymbol{\theta}) \left(\prod_{t=1}^{T-1} \frac{f(\mathbf{x}_t | \mathbf{x}_{t-1}, \boldsymbol{\theta}) g(\mathbf{y}_t | \mathbf{x}_t, \boldsymbol{\theta})}{\tilde{p}(\mathbf{x}_{t-1} | \boldsymbol{\theta}, \mathbf{x}_t, \mathbf{y}_{1:t})} \right) \frac{f(\mathbf{x}_T | \mathbf{x}_{T-1}, \boldsymbol{\theta}) g(\mathbf{y}_T | \mathbf{x}_T, \boldsymbol{\theta})}{\tilde{p}(\mathbf{x}_T, \boldsymbol{\theta}, \mathbf{x}_{T-1} | \mathbf{y}_{1:T})}. \end{aligned}$$

We summarize the smoothing procedure in Alg. 4.

Algorithm 4: Particle smoothing sampler accompanying Alg. 2.

- (a) Generate samples $\{\mathbf{X}_T^{(i)}, \Theta^{(i)}, \mathbf{X}_{T-1}^{(i)}\}_{i=1}^N$ from $\tilde{p}(\mathbf{x}_T, \boldsymbol{\theta}, \mathbf{x}_{t-1} | \mathbf{y}_{1:T})$ using \mathcal{F}_T^l .
 - (b) For $t = T-1, \dots, 1$, do the following
 - For each of $\{\Theta^{(i)}, \mathbf{X}_{t:T}^{(i)}\}_{i=1}^N$, invert the last block of \mathcal{F}_t^l as in (3.13) to generate a new sample $\mathbf{X}_{t-1}^{(i)}$.
 - (c) For each of $\{\Theta^{(i)}, \mathbf{X}_{0:T}^{(i)}\}_{i=1}^N$, compute the weight $W^{(i)}$ using (3.14).
 - (d) Normalize the weights as $W^{(i)} \leftarrow W^{(i)} / \sum_{i=1}^N W^{(i)}$.
-

The set of weighted samples $\{\Theta^{(i)}, \mathbf{X}_{0:T}^{(i)}, W^{(i)}\}_{i=1}^N$ is an unbiased representation of the joint posterior random variables $\boldsymbol{\Theta}, \mathbf{X}_{0:T} | \mathbf{y}_{1:T}$. It mitigates the particle degeneracy because the samples are drawn conditioned all observed data $\mathbf{y}_{1:T}$.

4. Error analysis. In this section we present how the error is accumulated in Alg. 2. We prove in Lemma 4.1 that in each iteration of Alg. 2, the Hellinger distance between the normalized densities is bounded by the L^2 distance between the square roots of their corresponding unnormalized densities. Then our analysis focuses on the accumulation of this L^2 error over time.

We define the unnormalized joint posterior density recursively as

$$\pi(\mathbf{x}_t, \boldsymbol{\theta}, \mathbf{x}_{t-1} | \mathbf{y}_{1:t}) = \int \pi(\mathbf{x}_{t-1}, \boldsymbol{\theta}, \mathbf{x}_{t-2} | \mathbf{y}_{1:t-1}) d\mathbf{x}_{t-2} f(\mathbf{x}_t | \mathbf{x}_{t-1}, \boldsymbol{\theta}) g(\mathbf{y}_t | \mathbf{x}_t, \boldsymbol{\theta}),$$

with $\pi(\mathbf{x}_1, \boldsymbol{\theta}, \mathbf{x}_0 | \mathbf{y}_1) = p(\boldsymbol{\theta}) p(\mathbf{x}_0 | \boldsymbol{\theta}) f(\mathbf{x}_1 | \mathbf{x}_0, \boldsymbol{\theta}) g(\mathbf{y}_1 | \mathbf{x}_1, \boldsymbol{\theta})$. Then (2.1) leads to the normalizing constant $z_t := \int \pi(\mathbf{x}_t, \boldsymbol{\theta}, \mathbf{x}_{t-1} | \mathbf{y}_{1:t}) d\mathbf{x}_t d\boldsymbol{\theta} d\mathbf{x}_{t-1} = p(\mathbf{y}_{1:t})$ and thus

$$p(\mathbf{x}_t, \boldsymbol{\theta}, \mathbf{x}_{t-1} | \mathbf{y}_{1:t}) = \frac{1}{z_t} \pi(\mathbf{x}_t, \boldsymbol{\theta}, \mathbf{x}_{t-1} | \mathbf{y}_{1:t}).$$

In the following analysis, we use shorthands $p_t(\mathbf{x}_t, \boldsymbol{\theta}, \mathbf{x}_{t-1}) := p(\mathbf{x}_t, \boldsymbol{\theta}, \mathbf{x}_{t-1} | \mathbf{y}_{1:t})$ and $\tilde{p}_t(\mathbf{x}_t, \boldsymbol{\theta}, \mathbf{x}_{t-1}) := \tilde{p}(\mathbf{x}_t, \boldsymbol{\theta}, \mathbf{x}_{t-1} | \mathbf{y}_{1:t})$ to denote the joint posterior density at time t and its tensor-train-based approximation, respectively. Similar notation is adopted to represent the unnormalized counterparts of these densities. We also omit the input variables when no confusion arises. Using this notation, we prove the following lemma.

LEMMA 4.1. *In each iteration of Alg. 2, the Hellinger distance between p_t and \tilde{p}_t is bounded by the L_2 distance between $\sqrt{\pi_t}$ and $\sqrt{\tilde{\pi}_t}$,*

$$D_H(p_t, \tilde{p}_t) \leq \frac{\sqrt{2}}{\sqrt{z_t}} \|\sqrt{\pi_t} - \sqrt{\tilde{\pi}_t}\|_{L^2}.$$

Proof. Note that $\|\sqrt{\pi_t}\|_{L^2} = \sqrt{z_t}$ and $\|\sqrt{\tilde{\pi}_t}\|_{L^2} = \sqrt{\tilde{z}_t}$. Applying the Cauchy-Schwarz inequality and triangle inequality, we have

$$\begin{aligned} |\tilde{z}_t - z_t| &\leq \|\pi_t - \tilde{\pi}_t\|_{L^1} = \|(\sqrt{\pi_t} - \sqrt{\tilde{\pi}_t})(\sqrt{\pi_t} + \sqrt{\tilde{\pi}_t})\|_{L^1} \\ &\leq \|\sqrt{\pi_t} - \sqrt{\tilde{\pi}_t}\|_{L^2} \|\sqrt{\pi_t} + \sqrt{\tilde{\pi}_t}\|_{L^2} \\ &\leq \|\sqrt{\pi_t} - \sqrt{\tilde{\pi}_t}\|_{L^2} (\|\sqrt{\pi_t}\|_{L^2} + \|\sqrt{\tilde{\pi}_t}\|_{L^2}) \\ (4.1) \quad &= \|\sqrt{\pi_t} - \sqrt{\tilde{\pi}_t}\|_{L^2} (\sqrt{z_t} + \sqrt{\tilde{z}_t}). \end{aligned}$$

Furthermore, using the identity $|\tilde{z}_t - z_t| = |\sqrt{\tilde{z}_t} - \sqrt{z_t}|(\sqrt{\tilde{z}_t} + \sqrt{z_t})$, the inequality in (4.1) leads to

$$(4.2) \quad |\sqrt{\tilde{z}_t} - \sqrt{z_t}| \leq \|\sqrt{\pi_t} - \sqrt{\tilde{\pi}_t}\|_{L^2}.$$

The Hellinger distance $D_H(p_t, \tilde{p}_t)$ satisfies

$$\begin{aligned} D_H(p_t, \tilde{p}_t) &= \frac{1}{\sqrt{2}} \left\| \frac{\sqrt{\pi_t}}{\sqrt{z_t}} - \frac{\sqrt{\tilde{\pi}_t}}{\sqrt{\tilde{z}_t}} \right\|_{L^2} \\ &= \frac{1}{\sqrt{2}} \left\| \frac{\sqrt{\pi_t}}{\sqrt{z_t}} - \frac{\sqrt{\tilde{\pi}_t}}{\sqrt{z_t}} + \frac{\sqrt{\tilde{\pi}_t}}{\sqrt{z_t}} - \frac{\sqrt{\tilde{\pi}_t}}{\sqrt{\tilde{z}_t}} \right\|_{L^2} \\ &\leq \frac{1}{\sqrt{2}} \left\| \frac{\sqrt{\pi_t}}{\sqrt{z_t}} - \frac{\sqrt{\tilde{\pi}_t}}{\sqrt{z_t}} \right\|_{L^2} + \frac{1}{\sqrt{2}} \left\| \frac{\sqrt{\tilde{\pi}_t}}{\sqrt{z_t}} - \frac{\sqrt{\tilde{\pi}_t}}{\sqrt{\tilde{z}_t}} \right\|_{L^2} \\ &= \frac{\|\sqrt{\pi_t} - \sqrt{\tilde{\pi}_t}\|_{L^2}}{\sqrt{2z_t}} + \frac{\|\sqrt{\tilde{\pi}_t}\|_{L^2}}{\sqrt{2}} \left| \frac{1}{\sqrt{z_t}} - \frac{1}{\sqrt{\tilde{z}_t}} \right| \\ &= \frac{\|\sqrt{\pi_t} - \sqrt{\tilde{\pi}_t}\|_{L^2}}{\sqrt{2z_t}} + \frac{1}{\sqrt{2z_t}} |\sqrt{\tilde{z}_t} - \sqrt{z_t}|. \end{aligned}$$

Then, applying (4.2), we have

$$(4.3) \quad D_H(p_t, \tilde{p}_t) \leq \frac{\sqrt{2}}{\sqrt{z_t}} \|\sqrt{\pi_t} - \sqrt{\tilde{\pi}_t}\|_{L^2}. \quad \square$$

Using the above lemma, it is sufficient for us to consider the accumulation of $\|\sqrt{\pi_t} - \sqrt{\tilde{\pi}_t}\|_{L^2}$. Recall in each of the iterations of Alg. 2, the unnormalized joint posterior density $\pi_t(\mathbf{x}_t, \boldsymbol{\theta}, \mathbf{x}_{t-1})$ can not be directly evaluated since it takes the marginal form. Instead, we introduce the intermediate unnormalized approximation $\hat{\pi}_t(\mathbf{x}_t, \boldsymbol{\theta}, \mathbf{x}_{t-1})$, and then approximate it using the tensor train $\tilde{\pi}_t(\mathbf{x}_t, \boldsymbol{\theta}, \mathbf{x}_{t-1})$ in (3.8). One can evaluate the intermediate unnormalized density

$$\hat{\pi}_t(\mathbf{x}_t, \boldsymbol{\theta}, \mathbf{x}_{t-1}) = \tilde{\pi}(\mathbf{x}_{t-1}, \boldsymbol{\theta} | \mathbf{y}_{1:t-1}) f(\mathbf{x}_t | \mathbf{x}_{t-1}, \boldsymbol{\theta}) g(\mathbf{y}_t | \mathbf{x}_t, \boldsymbol{\theta}),$$

that is constructed from the previous approximation $\tilde{\pi}(\mathbf{x}_{t-1}, \boldsymbol{\theta} | \mathbf{y}_{1:t-1})$, as shown in step (a) of Alg. 2. The intermediate approximation enables pointwise function evaluations used for building the tensor-train-based approximation $\tilde{\pi}(\mathbf{x}_t, \boldsymbol{\theta}, \mathbf{x}_{t-1} | \mathbf{y}_{1:t})$.

This leads to a two-step approximation procedure in Alg. 2. The joint density $\pi_t(\mathbf{x}_t, \boldsymbol{\theta}, \mathbf{x}_{t-1})$ is approximated by the intermediate density $\hat{\pi}_t(\mathbf{x}_t, \boldsymbol{\theta}, \mathbf{x}_{t-1})$, and then the tensor-train-based approximation $\tilde{\pi}_t(\mathbf{x}_t, \boldsymbol{\theta}, \mathbf{x}_{t-1})$ is constructed from the intermediate density $\hat{\pi}_t(\mathbf{x}_t, \boldsymbol{\theta}, \mathbf{x}_{t-1})$ using the squared-tensor-train approximation outlined in Section 3.1. The errors are accumulated as follows. In the previous iteration, the joint posterior density $\pi_{t-1}(\mathbf{x}_{t-1}, \boldsymbol{\theta}, \mathbf{x}_{t-2})$ has the approximation $\tilde{\pi}_{t-1}(\mathbf{x}_{t-1}, \boldsymbol{\theta}, \mathbf{x}_{t-2})$. The corresponding approximation error is propagated into the new intermediate approximation $\hat{\pi}_t(\mathbf{x}_t, \boldsymbol{\theta}, \mathbf{x}_{t-1})$ through the marginalized approximation $\tilde{\pi}(\mathbf{x}_{t-1}, \boldsymbol{\theta} | \mathbf{y}_{1:t-1})$. Then, a second error is incurred during the tensor-train approximation of the square root $\sqrt{\hat{\pi}_t(\mathbf{x}_t, \boldsymbol{\theta}, \mathbf{x}_{t-1})}$.

This way, we can decompose $\|\sqrt{\pi_t} - \sqrt{\tilde{\pi}_t}\|_{L^2}$ using the triangle inequality

$$(4.4) \quad \|\sqrt{\pi_t} - \sqrt{\tilde{\pi}_t}\|_{L^2} \leq \|\sqrt{\pi_t} - \sqrt{\hat{\pi}_t}\|_{L^2} + \|\hat{\pi}_t - \sqrt{\tilde{\pi}_t}\|_{L^2},$$

where $\|\sqrt{\pi_t} - \sqrt{\hat{\pi}_t}\|_{L^2}$ measures the propagation error from the previous iteration, while $\|\hat{\pi}_t - \sqrt{\tilde{\pi}_t}\|_{L^2}$ measures the tensor-train approximation error in the current iteration. The tensor-train approximation error $\|\hat{\pi}_t - \sqrt{\tilde{\pi}_t}\|_{L^2}$ can be directly bounded using Lemma 3.1. In the following, Proposition 4.2 establishes the propagation error $\|\sqrt{\pi_t} - \sqrt{\hat{\pi}_t}\|_{L^2}$ at time t . Then, Theorem 4.3 provides a bound on the total error $\|\sqrt{\pi_t} - \sqrt{\tilde{\pi}_t}\|_{L^2}$ and Corollary 4.4 provides a bound on the accumulated Hellinger error of the approximation over time.

PROPOSITION 4.2. *Assume either of the following bounds holds*

$$(4.5) \quad C_t^{(g)} = \sup_{\mathbf{x}_t \in \mathcal{X}, \boldsymbol{\theta} \in \Theta} g(\mathbf{y}_t | \mathbf{x}_t, \boldsymbol{\theta}) < \infty,$$

$$(4.6) \quad C_t^{(f)} = \sup_{\mathbf{x}_{t-1} \in \mathcal{X}, \boldsymbol{\theta} \in \Theta} \int f(\mathbf{x}_t | \mathbf{x}_{t-1}, \boldsymbol{\theta}) g(\mathbf{y}_t | \mathbf{x}_t, \boldsymbol{\theta}) d\mathbf{x}_t < \infty.$$

Then the propagation error $\|\sqrt{\pi_t} - \sqrt{\hat{\pi}_t}\|_{L^2}$ in time t is bounded by

$$(4.7) \quad \|\sqrt{\pi_t} - \sqrt{\hat{\pi}_t}\|_{L^2} \leq \sqrt{C_t^{(h)}} \|\sqrt{\pi_{t-1}} - \sqrt{\tilde{\pi}_{t-1}}\|_{L^2}$$

where $h \in \{f, g\}$.

Proof. Recall that the unnormalized intermediate density takes the form

$$\hat{\pi}_t(\mathbf{x}_t, \boldsymbol{\theta}, \mathbf{x}_{t-1}) = \tilde{\pi}(\mathbf{x}_{t-1}, \boldsymbol{\theta} | \mathbf{y}_{1:t-1}) f(\mathbf{x}_t | \mathbf{x}_{t-1}, \boldsymbol{\theta}) g(\mathbf{y}_t | \mathbf{x}_t, \boldsymbol{\theta}).$$

Then the squared propagation error can be expressed as

$$(4.8) \quad \begin{aligned} & \|\sqrt{\pi_t} - \sqrt{\hat{\pi}_t}\|_{L^2}^2 \\ &= \int \left(\sqrt{\pi(\mathbf{x}_{t-1}, \boldsymbol{\theta} | \mathbf{y}_{1:t-1})} - \sqrt{\tilde{\pi}(\mathbf{x}_{t-1}, \boldsymbol{\theta} | \mathbf{y}_{1:t-1})} \right)^2 r(\mathbf{x}_{t-1}, \boldsymbol{\theta}) d\mathbf{x}_{t-1} d\boldsymbol{\theta} \end{aligned}$$

where $r(\mathbf{x}_{t-1}, \boldsymbol{\theta}) = \int f(\mathbf{x}_t | \mathbf{x}_{t-1}, \boldsymbol{\theta}) g(\mathbf{y}_t | \mathbf{x}_t, \boldsymbol{\theta}) d\mathbf{x}_t$. Either assumption (4.5) or (4.6) leads to

$$\sup_{\mathbf{x}_{t-1} \in \mathcal{X}, \boldsymbol{\theta} \in \Theta} r(\mathbf{x}_{t-1}, \boldsymbol{\theta}) \leq C_t^{(h)}, \quad h \in \{f, g\}.$$

Then, we have

$$\begin{aligned}\|\sqrt{\pi_t} - \sqrt{\hat{\pi}_t}\|_{L^2}^2 &\leq C_t^{(h)} \int \left(\sqrt{\pi(\mathbf{x}_{t-1}, \boldsymbol{\theta} | \mathbf{y}_{1:t-1})} - \sqrt{\tilde{\pi}(\mathbf{x}_{t-1}, \boldsymbol{\theta} | \mathbf{y}_{1:t-1})} \right)^2 d\mathbf{x}_{t-1} d\boldsymbol{\theta} \\ &= C_t^{(h)} \left\| \sqrt{\pi(\mathbf{x}_{t-1}, \boldsymbol{\theta} | \mathbf{y}_{1:t-1})} - \sqrt{\tilde{\pi}(\mathbf{x}_{t-1}, \boldsymbol{\theta} | \mathbf{y}_{1:t-1})} \right\|_{L^2}^2.\end{aligned}$$

Applying Lemma A.2, the L_2 distance for the marginal densities is bounded by that for the joint densities as

$$\left\| \sqrt{\pi(\mathbf{x}_{t-1}, \boldsymbol{\theta} | \mathbf{y}_{1:t-1})} - \sqrt{\tilde{\pi}(\mathbf{x}_{t-1}, \boldsymbol{\theta} | \mathbf{y}_{1:t-1})} \right\|_{L^2} \leq \|\sqrt{\pi_{t-1}} - \sqrt{\tilde{\pi}_{t-1}}\|_{L^2}$$

Taking square root of both sides of the above equation gives the desired result. \square

THEOREM 4.3. *In each iteration of Alg. 2, suppose the tensor-train approximation ϕ_t has an L_2 error that satisfies $\|\phi_t - \sqrt{\hat{\pi}_t}\|_{L^2} < \epsilon_t$ and the constant $\tau \leq \|\phi_t - \sqrt{\hat{\pi}_t}\|_{L^2}^2$. Suppose further one of the assumptions of Proposition 4.2 holds. For $t > 0$, we have*

$$\|\sqrt{\pi_t} - \sqrt{\tilde{\pi}_t}\|_{L^2} \leq \sqrt{C_t^{(h)}} \|\sqrt{\pi_{t-1}} - \sqrt{\tilde{\pi}_{t-1}}\|_{L^2} + \sqrt{2} \epsilon_t, \quad h \in \{f, g\}.$$

Proof. The result follows from the triangle inequality (4.4). We bound the propagation error $\|\sqrt{\pi_t} - \sqrt{\hat{\pi}_t}\|_{L^2}$ using Proposition 4.2. The approximation error $\|\sqrt{\hat{\pi}_t} - \sqrt{\tilde{\pi}_t}\|_{L^2}$ is bounded by Lemma 3.1. \square

COROLLARY 4.4. *Suppose the conditions of Theorem 4.3 hold and there exists a constant C such that $C = \sup_t C_t^{(h)} < \infty$ for $t > 0$ and $h \in \{f, g\}$. Then the Hellinger distance between p_t and its tensor-train approximation \tilde{p}_t is bounded by*

$$D_H(p_t, \tilde{p}_t) \leq \frac{2}{\sqrt{p(\mathbf{y}_{1:t})}} \sum_{k=1}^t C^{k-j} \epsilon_k.$$

Proof. Firstly we recall that there is no approximation used in Alg. 2 at t_0 , as we only have the prior for \mathbf{X}_0 and $\boldsymbol{\Theta}$. This way, i.e., $\epsilon_0 = 0$. Applying Theorem 4.3, by induction we have

$$(4.9) \quad \|\sqrt{\pi_t} - \sqrt{\tilde{\pi}_t}\|_{L^2} \leq \sqrt{2} \sum_{k=1}^t C^{k-j} \epsilon_k.$$

Substituting (4.9) and $z_t = p(\mathbf{y}_{1:t})$ into Lemma 4.1, we complete the proof. \square

Note that (4.8) in the proof of Proposition 4.2 reveals the fact that the propagated L^2 error can be considered as a “weighted” L^2 error of the previous approximation under the function $r(\mathbf{x}_{t-1}, \boldsymbol{\theta})$. Assumptions of Proposition 4.2 is usually satisfied in practice. For example, an observation model with the commonly used Gaussian noise leads to a constant $C_t^{(g)} = 1$. In this case, the Hellinger error in Corollary 4.4 is a linear combination of approximation errors. In Section 6, we observe that the Hellinger error accumulates linearly in time in most the numerical experiments.

Remark 4.5. The state and parameter densities of interest in (1.5) and (1.6) are both marginal form of $p(\mathbf{x}_t, \boldsymbol{\theta}, \mathbf{x}_{t-1} | \mathbf{y}_{1:t})$. By Lemma A.1, we know that Hellinger distance between marginals and their corresponding tensor-train approximations can not exceed the Hellinger error between joint densities presented in Corollary 4.4.

5. Preconditioning methods. The posterior densities with complex nonlinear interactions between parameters and states are ubiquitous in practice and lead to high-rank tensor-train approximation in step (b) of Alg. 2. This will dramatically increase the computational complexity to achieve sufficient accuracy; recall that squared-tensor-train construction requires $\sum_{k=1}^m r_k^2$ evaluations of the target density. In this section, we present preconditioning methods to reduce the tensor-train ranks and refine the estimation algorithm with preconditioner.

Assume we aim to characterize $\mathbf{X} \in \mathbb{R}^m$ whose density $p_{\mathbf{X}}(\mathbf{x})$ can not be efficiently approximated using the tensor train. Let \mathcal{L} denote a lower-triangular transport map from $\mathbf{V} \in \mathbb{R}^m$ to $\mathbf{Z} \in \mathbb{R}^m$ with densities $p_{\mathbf{V}}(\mathbf{v})$ and $p_{\mathbf{Z}}(\mathbf{z})$ respectively,

$$(5.1) \quad \mathbf{z} = \mathcal{L}(\mathbf{v}) = [\mathcal{L}^{(1)}(v_1), \mathcal{L}^{(2)}(\mathbf{v}_{1:2}), \dots, \mathcal{L}^{(m)}(\mathbf{v}_{1:m})]^\top, \quad p_{\mathbf{Z}}(\mathbf{z}) = \mathcal{L}_\# p_{\mathbf{V}}(\mathbf{z}),$$

such that each map $v_k \mapsto \mathcal{L}^{(k)}(\mathbf{v}_{1:k-1}, v_k)$ is homeomorphic, strictly increasing and differentiable in v_k . Assume further we can compute the marginal densities of \mathbf{V} and \mathbf{Z} and thus establish the corresponding KR rearrangement. Then we can use \mathcal{L} as a preconditioner to precondition the density of \mathbf{X} and instead approximate

$$(5.2) \quad q(\mathbf{v}) = \mathcal{L}^\# p_{\mathbf{X}}(\mathbf{v})$$

with the defensive squared-tensor-train approximation denoted by $\tilde{q}(\mathbf{v})$ as in (3.1). Recall this also facilitates the corresponding lower-triangular KR rearrangement $\mathcal{F}^l : \mathbb{R}^m \mapsto [0, 1]^m$, which transforms $\mathbf{V}' \sim \tilde{q}(\mathbf{v})$ into a uniform random variable $\mathbf{U} = \mathcal{F}^l(\mathbf{V}')$ with $\mathbf{U} \sim \text{Uni}(\mathbf{u}; [0, 1]^m)$. The choice of \mathcal{L} will be discussed later. Now we apply the change-of-variable chain as follows

$$\mathbf{u} \xrightarrow{\mathcal{F}^{-1}} \mathbf{v} \xrightarrow{\mathcal{L}} \mathbf{x}.$$

Then the following proposition gives the densities under \mathcal{L} and \mathcal{F} .

PROPOSITION 5.1. *Consider the preconditioner \mathcal{L} defined in (5.1). The pullback density $q(\mathbf{v})$ defined in (5.2) and its pushforward counterpart satisfy*

$$(5.3) \quad q(\mathbf{v}) = p_{\mathbf{X}}(\mathcal{L}(\mathbf{v})) \frac{p_{\mathbf{V}}(\mathbf{v})}{p_{\mathbf{Z}}(\mathcal{L}(\mathbf{v}))} \quad \text{and} \quad p_{\mathbf{X}}(\mathbf{x}) = q(\mathcal{L}^{-1}(\mathbf{x})) \frac{p_{\mathbf{Z}}(\mathbf{x})}{p_{\mathbf{V}}(\mathcal{L}^{-1}(\mathbf{x}))}.$$

The pushforward density of $p_{\mathbf{U}}(\mathbf{u})$ under the composition of \mathcal{L} and the squared-tensor-train induced lower-triangular map $(\mathcal{F}^l)^{-1}$ satisfies

$$(5.4) \quad \tilde{p}_{\mathbf{X}}(\mathbf{x}) := (\mathcal{L} \circ (\mathcal{F}^l)^{-1})_\# p_{\mathbf{U}}(\mathbf{x}) = \tilde{q}(\mathcal{L}^{-1}(\mathbf{x})) \frac{p_{\mathbf{Z}}(\mathbf{x})}{p_{\mathbf{V}}(\mathcal{L}^{-1}(\mathbf{x}))}.$$

Furthermore, the composition $\mathcal{L} \circ (\mathcal{F}^l)^{-1}$ is lower-triangular.

Proof. Since $p_{\mathbf{Z}}(\mathbf{z}) = \mathcal{L}_\# p_{\mathbf{V}}(\mathbf{z})$, we have

$$(5.5) \quad |\nabla_{\mathbf{v}} \mathcal{L}(\mathbf{v})| = \frac{p_{\mathbf{V}}(\mathbf{v})}{p_{\mathbf{Z}}(\mathcal{L}(\mathbf{v}))} \quad \text{and} \quad |\nabla_{\mathbf{z}} \mathcal{L}^{-1}(\mathbf{z})| = \frac{p_{\mathbf{Z}}(\mathbf{z})}{p_{\mathbf{V}}(\mathcal{L}^{-1}(\mathbf{z}))}.$$

Then (5.3) directly follows from $q(\mathbf{v}) = \mathcal{L}^\# p_{\mathbf{X}}(\mathbf{v})$ and $p_{\mathbf{X}}(\mathbf{x}) = \mathcal{L}_\# q_{\mathbf{V}}(\mathbf{x})$. To derive $\tilde{p}_{\mathbf{X}}(\mathbf{x})$, let $\mathbf{v} = \mathcal{L}^{-1}(\mathbf{x})$ and $\mathbf{u} = \mathcal{F}^l(\mathbf{v})$. Note $|\nabla_{\mathbf{v}} \mathcal{F}^l(\mathbf{v})| = \tilde{q}(\mathbf{v})$, we have

$$(\mathcal{L} \circ (\mathcal{F}^l)^{-1})_\# p_{\mathbf{U}}(\mathbf{x}) = p_{\mathbf{U}}(\mathcal{F}^l \circ \mathcal{L}^{-1}(\mathbf{x})) |\nabla_{\mathbf{x}} \mathcal{F}^l \circ \mathcal{L}^{-1}(\mathbf{x})|$$

$$\begin{aligned}
&= |\nabla_{\mathbf{v}} \mathcal{F}^l(\mathbf{v})| |\nabla_{\mathbf{x}} \mathcal{L}^{-1}(\mathbf{x})| \\
&= \tilde{q}(\mathbf{v}) \frac{p_{\mathbf{Z}}(\mathbf{x})}{p_{\mathbf{V}}(\mathbf{v})}
\end{aligned}$$

Substituting $\mathbf{v} = \mathcal{L}^{-1}(\mathbf{x})$, we obtain (5.4). Furthermore, since \mathcal{L} and $(\mathcal{F}^l)^{-1}$ are lower-triangular by construction, their composition $\mathcal{L} \circ (\mathcal{F}^l)^{-1}$ is also lower-triangular. \square

Proposition 5.1 indicates the target density $p_{\mathbf{X}}(\mathbf{x})$ is approximated by $\tilde{p}_{\mathbf{X}}(\mathbf{x})$, since $q(\mathbf{v}) \approx \tilde{q}(\mathbf{v})$. Recall the cornerstone of recursive Bayesian inference in state space model is to integrate the joint densities. The lower triangularity of \mathcal{L} and $(\mathcal{F}^l)^{-1}$ also gives rise to the approximate marginal density $\tilde{p}(\mathbf{x}_{1:k}) = \int \tilde{p}_{\mathbf{X}}(\mathbf{x}) d\mathbf{x}_{k+1:m}$. Let

$$\mathcal{L}^{(1:k)}(\mathbf{v}_{1:k}) = [\mathcal{L}^{(1)}(v_1), \dots, \mathcal{L}^{(k)}(\mathbf{v}_{1:k})]^\top,$$

and similarly for $\mathcal{F}^{l(1:k)}(\mathbf{x}_{1:k})$. Note $\tilde{q}(\mathbf{v})$ is a squared tensor train and its integration $\tilde{q}_{1:k}(\mathbf{v}_{1:k}) = \int \tilde{q}(\mathbf{v}_{1:m}) d\mathbf{v}_{k+1:m}$ can be computed from Proposition 3.2. Then following the same reasoning as the proof of Proposition 5.1, we have

$$\begin{aligned}
(5.6) \quad \tilde{p}(\mathbf{x}_{1:k}) &= (\mathcal{L}^{(1:k)} \circ (\mathcal{F}^{l(1:k)})^{-1})_{\#} p_{U_{1:k}}(\mathbf{x}_{1:k}) \\
&= \tilde{q}_{1:k}((\mathcal{L}^{(1:k)})^{-1}(\mathbf{x}_{1:k})) \frac{p_{\mathbf{Z}_{1:k}}(\mathbf{x}_{1:k})}{p_{\mathbf{V}_{1:k}}((\mathcal{L}^{(1:k)})^{-1}(\mathbf{x}_{1:k}))}.
\end{aligned}$$

The conditional densities also naturally follow as in Section 3.1.

When only the unnormalized density $\pi(\mathbf{x}) = z p_{\mathbf{X}}(\mathbf{x})$ is available, (5.3) still holds except that $q(\mathbf{u})$ here is not a normalized density. Correspondingly $\tilde{p}(\mathbf{x}_{1:k})$ in (5.6) is replaced by $\tilde{\pi}(\mathbf{x}_{1:k})$. We can still apply the above procedure and approximate z using $\tilde{z} = \int \tilde{q}(\mathbf{v}) d\mathbf{v}$. As a result, we can precondition the approximate density $\tilde{\pi}(\mathbf{x}_t, \boldsymbol{\theta}, \mathbf{x}_{t-1} | \mathbf{y}_{1:t})$ in Alg. 2 and obtain the following algorithm.

Algorithm 5: Sequential estimation with preconditioning.

- (a) At time t , given the intermediate approximation $\hat{\pi}(\mathbf{x}_t, \boldsymbol{\theta}, \mathbf{x}_{t-1} | \mathbf{y}_{t-1})$ in step (a) of Alg. 2 and the preconditioner \mathcal{L}_t , we can establish the squared tensor train $\tilde{q}_t(\mathbf{v}_t, \mathbf{v}_\theta, \mathbf{v}_{t-1})$ following (5.3) with $p_{\mathbf{X}}(\mathbf{x})$ substituted by $\hat{\pi}(\mathbf{x}_t, \boldsymbol{\theta}, \mathbf{x}_{t-1} | \mathbf{y}_{t-1})$.
- (b) Apply (5.6) for $k = m + d$ to obtain $\tilde{\pi}(\mathbf{x}_t, \boldsymbol{\theta} | \mathbf{y}_{1:t})$.

In the next time step $t+1$, we can apply the same procedure using the newly computed marginal approximation $\tilde{\pi}(\mathbf{x}_t, \boldsymbol{\theta} | \mathbf{y}_{1:t})$.

Remark 5.2. The smoother with preconditioning can be accordingly modified from Alg. 4 and we omit the details here. For the auxiliary particle filter in Alg. 3, one need to compute $\mathcal{F}_t^u(\mathbf{x}_t | \boldsymbol{\theta}, \mathbf{x}_{t-1})$, which requires computing $\int \tilde{\pi}(\mathbf{x}_t, \boldsymbol{\theta}, \mathbf{x}_{t-1} | \mathbf{y}_{1:t}) d\mathbf{x}_t$. This can be achieved by forcing the lower-triangular map \mathcal{L} to also be upper-triangular and thus diagonal. Then the resulting composition $\mathcal{L} \circ (\mathcal{F}_t^u)^{-1}$ is upper-triangular. Following similar reasoning as above we obtain the auxiliary particle filter with preconditioning.

Then it remains to choose an efficient preconditioner \mathcal{L} . The preconditioner usually varies for different target densities and need to be computed in each iteration. Thus in Alg. 5 the preconditioner \mathcal{L}_t varies along time. The work in [3] shows that such \mathcal{L} is unique given any pair of \mathbf{V} and \mathbf{Z} . In our work, \mathbf{V} is just some simple independent reference random variables such as standard Gaussian or uniform. Thus the characterization of \mathcal{L} is equivalent to the characterization of \mathbf{Z} . In the idealized scenario that $\mathbf{Z} = \mathbf{X}$, we have the pullback density in (5.3) follows $q(\mathbf{v}) = p_{\mathbf{V}}(\mathbf{v})$,

which is a rank-one tensor train by assumption. In practice, an efficient preconditioner should be able to capture part of the structure of the target \mathbf{X} . We suggest two types of preconditioners in the rest of this section, both of which prove efficient in Sec 6.

5.1. Linear preconditioning. Linear preconditioning is one of the simplest preconditioning methods and only captures the location and the range of the target density $\hat{\pi}(\mathbf{x}_t, \boldsymbol{\theta}, \mathbf{x}_{t-1} | \mathbf{y}_{1:t})$. The map \mathcal{L}_t is defined to be

$$[\mathbf{x}_t, \boldsymbol{\theta}, \mathbf{x}_{t-1}]^\top = \mathcal{L}_t(\mathbf{u}_t, \mathbf{u}_\theta, \mathbf{u}_{t-1}) := \mathbf{L}_t[\mathbf{u}_t, \mathbf{u}_\theta, \mathbf{u}_{t-1}]^\top + \boldsymbol{\mu}_t,$$

where ideally $\boldsymbol{\mu}_t$ is the expectation of $\mathbf{X}_t, \boldsymbol{\Theta}, \mathbf{X}_{t-1} | \mathbf{y}_{1:t}$ and \mathbf{L}_t is the Cholesky decomposition of its covariance. Then the (unnormalized) pullback density $q_t(\mathbf{v}_t, \mathbf{v}_\theta, \mathbf{v}_{t-1})$ is centred with identity covariance matrix.

However, in practice the expectation and the variance of the posterior density is intractable. But we can obtain an approximation of these statistics using an one-step particle filter. Suppose at time $t-1$, we have the the squared-tensor-train approximation $\tilde{q}_{t-1}(\mathbf{x}_{t-1}, \boldsymbol{\theta}, \mathbf{x}_{t-2})$ and the preconditioner L_{t-1} . Applying Proposition 5.1, we have

$$[\mathbf{X}_{t-1}, \boldsymbol{\Theta}, \mathbf{X}_{t-2}] = \mathcal{L}_{t-1} \circ (\mathcal{F}_{t-1}^l)^{-1}(\mathbf{U}_{t-1}, \mathbf{U}_\theta, \mathbf{U}_{t-2})$$

following $\tilde{\pi}(\mathbf{x}_{t-1}, \boldsymbol{\theta}, \mathbf{x}_{t-2} | \mathbf{y}_{1:t-1})$, where $\mathbf{U}_{t-1}, \mathbf{U}_\theta, \mathbf{U}_{t-2}$ are independent uniform random variables. Then we can generate a set of samples $\{\mathbf{X}_{t-1}^{(i)}, \boldsymbol{\Theta}^{(i)}, \mathbf{X}_{t-2}^{(i)}\}_{i=1}^N$ following $\tilde{\pi}(\mathbf{x}_{t-1}, \boldsymbol{\theta}, \mathbf{x}_{t-2} | \mathbf{y}_{1:t-1})$ and then propagate it to time t using $f(\mathbf{x}_t | \mathbf{x}_{t-1}, \boldsymbol{\theta})$ and reweight it using $g(\mathbf{y}_t | \mathbf{x}_t, \boldsymbol{\theta})$. We end up with $\{\mathbf{X}_t^{(i)}, \mathbf{X}_{t-1}^{(i)}, \boldsymbol{\Theta}^{(i)}, \mathbf{W}_t^{(i)}\}_{i=1}^N$ following $\hat{\pi}(\mathbf{x}_t, \boldsymbol{\theta}, \mathbf{x}_{t-1} | \mathbf{y}_{1:t})$, from which we can use Monte Carlo method to approximate the expectation $\boldsymbol{\mu}_t$ and matrix \mathbf{L}_t .

Remark 5.3. Since the tensor-train approximate density $\tilde{p}(\mathbf{x}_t, \boldsymbol{\theta}, \mathbf{x}_{t-1} | \mathbf{y}_{1:t})$ is the pushforward density of q_t under the same map \mathcal{L}_t as in the preconditioning step, the error in the approximation of \mathbf{L}_t and $\boldsymbol{\mu}_t$ is automatically corrected. Thus a rough approximation of \mathbf{L}_t and $\boldsymbol{\mu}_t$ suffices. As a result, the number of particles in the one-step particle filter can remain small.

The linear preconditioning method occupies a privileged role in the preconditioning methods since it is necessary even in the basic version of our algorithm. Without the approximate location and range of the posterior density, we have to establish the tensor-train approximation in the unbounded domain, which leads to large approximation error. With linear preconditioner in each iteration, we can approximate the centred function q_t in the domain $[-c, c]$ for some constant c , uniformly in all the iterations.

Remark 5.4. We can further set \mathbf{L}_t to be diagonal, with the diagonal entries equal to the approximate standard deviation of $\mathbf{X}_t, \boldsymbol{\Theta}, \mathbf{X}_{t-1} | \mathbf{y}_{1:t}$ along each dimension. Then by Remark 5.2, the linear preconditioning method can be naturally incorporated to the particle filter in Alg. 3 and we can skip the above one-step particle filter.

5.2. Non-linear preconditioning. In state space models, the posterior density tends to be concentrated and involve non-linear dependency between parameters and states. Then only linear preconditioning is not enough to obtain the sufficient accuracy using tensor trains of decent ranks. To further enhance the tensor-train approximation power, we apply the KR rearrangement \mathcal{F}_{t-1}^l from the previous step $t-1$ to establish the non-linear preconditioner used at time t . Such preconditioner is efficient since

intuitively the posterior density is likely to remain steady over time and thus the posterior density at time $t - 1$ can capture the structure of that at time t .

For non-linear preconditioning methods, the variables of the density function need to be reordered as $(\boldsymbol{\theta}, \mathbf{x}_t, \mathbf{x}_{t-1})$ for the reasons explained later. We will no longer utilize \mathcal{F}^u in this section and thus let \mathcal{F}_{t-1} denote \mathcal{F}_{t-1}^l in the following analysis for brevity. We also set \mathbf{V} to be the uniform reference random variables as $\mathbf{V} \sim \text{Uni}(\mathbf{v}; [0, 1]^{2m+d})$.

Assume at time $t - 1$, we have the preconditioner \mathcal{L}_{t-1} , the squared-tensor-train approximation $\tilde{q}_{t-1}(\mathbf{v}_\theta, \mathbf{v}_{t-1}, \mathbf{v}_{t-2})$ and the induced lower-triangular KR rearrangement \mathcal{F}_{t-1} . Define $\mathcal{T}_{t-1} = \mathcal{L}_{t-1} \circ (\mathcal{F}_{t-1})^{-1}$. Then by Proposition 5.1, \mathcal{T}_{t-1} takes lower-triangular form

$$(\boldsymbol{\theta}, \mathbf{x}_{t-1}, \mathbf{x}_{t-2}) = \mathcal{T}_{t-1}(\mathbf{u}_\theta, \mathbf{u}_{t-1}, \mathbf{u}_{t-2}) = \begin{bmatrix} \mathcal{T}_{t-1}^{(\theta)}(\mathbf{u}_\theta) \\ \mathcal{T}_{t-1}^{(t-1)}(\mathbf{u}_\theta, \mathbf{u}_{t-1}) \\ \mathcal{T}_{t-1}^{(t-2)}(\mathbf{u}_\theta, \mathbf{u}_{t-1}, \mathbf{u}_{t-2}) \end{bmatrix}.$$

and $\tilde{p}(\mathbf{x}_\theta, \mathbf{x}_{t-1} | \mathbf{y}_{1:t-1}) = (\mathcal{T}_{t-1}^{(\theta, t-1)})_{\#} p_U(\mathbf{x}_\theta, \mathbf{x}_{t-1})$, where $\mathcal{T}_{t-1}^{(\theta, t-1)}$ denotes the first two blocks of \mathcal{T}_{t-1} .

At time t , recall the intermediate approximation takes the form

$$\hat{\pi}(\boldsymbol{\theta}, \mathbf{x}_t, \mathbf{x}_{t-1} | \mathbf{y}_{1:t}) = \tilde{\pi}_{t-1}(\boldsymbol{\theta}, \mathbf{x}_{t-1}) f(\mathbf{x}_t | \mathbf{x}_{t-1}, \boldsymbol{\theta}) g(\mathbf{y}_t | \mathbf{x}_t, \boldsymbol{\theta}).$$

We augment $\mathcal{T}_{t-1}^{(\theta, t-1)}$ to the preconditioner \mathcal{L}_t as

$$(5.7) \quad \mathcal{L}_t(\mathbf{u}_\theta, \mathbf{u}_t, \mathbf{u}_{t-1}) = \begin{bmatrix} \mathcal{T}_{t-1}^{(\theta)}(\mathbf{u}_\theta) \\ I_m(\quad, \mathbf{u}_t) \\ \mathcal{T}_{t-1}^{(t-1)}(\mathbf{u}_\theta, \quad, \mathbf{u}_{t-1}) \end{bmatrix},$$

where I denotes the identity map. It then follows that

$$(\mathcal{L}_t)_{\#} p_U(\mathbf{x}_\theta, \mathbf{x}_t, \mathbf{x}_{t-1}) = p_U(\mathbf{u}_t) (\mathcal{T}_{t-1}^{(\theta, t-1)})_{\#} p_U(\mathbf{x}_\theta, \mathbf{x}_{t-1}) = \tilde{p}(\mathbf{x}_\theta, \mathbf{x}_{t-1} | \mathbf{y}_{1:t-1}).$$

Then the pullback density $q_t(\mathbf{v}_\theta, \mathbf{v}_t, \mathbf{v}_{t-1})$ is obtained by substituting $\hat{\pi}$, p_U and \tilde{p} above into $p_{\mathbf{X}}$, $p_{\mathbf{V}}$ and $p_{\mathbf{Z}}$ in (5.3) respectively. Then following the procedure in Alg. 5, we obtain the lower-triangular map \mathcal{F}_t and thus $\mathcal{T}_t = \mathcal{L}_t \circ \mathcal{F}_t^{-1}$ as follows,

$$(5.8) \quad \mathcal{T}_t(\mathbf{u}_\theta, \mathbf{u}_t, \mathbf{u}_{t-1}) = \begin{bmatrix} \mathcal{T}_{t-1}^{(\theta)} \circ (\mathcal{F}_t^{-1})^{(\theta)}(\mathbf{u}_\theta) \\ (\mathcal{F}_t^{-1})^{(t)}(\mathbf{u}_\theta, \mathbf{u}_t) \\ \mathcal{T}_{t-1}^{(t-1)} \circ (\mathcal{F}_t^{-1})^{(t)}(\mathbf{u}_\theta, \mathbf{u}_t, \mathbf{u}_{t-1}) \end{bmatrix}.$$

The first two blocks of \mathcal{T}_t will contribute to the preconditioner in the next time step $t + 1$. This raises the problem of nested preconditioning as

$$(5.9) \quad \mathcal{T}_t^{(\theta)} = (\mathcal{F}_1^{-1})^{(\theta)} \circ \dots \circ (\mathcal{F}_t^{-1})^{(\theta)}(\mathbf{u}_\theta).$$

Consequently, the evaluation of q_t at time t needs to evaluate all the marginal squared tensor-train approximations up to time $t - 1$, which is computationally expensive. We collapse this map by establishing an auxiliary tensor-train approximation of $\tilde{p}(\boldsymbol{\theta} | \mathbf{y}_{1:t}) = \int \tilde{p}(\boldsymbol{\theta}, \mathbf{x}_t, \mathbf{x}_{t-1} | \mathbf{y}_{1:t}) d\mathbf{x}_t d\mathbf{x}_{t-1}$ in each step without preconditioning and obtain the KR rearrangement $\mathcal{S}_t : [0, 1]^d \mapsto \Theta$. This explains why we need to reorder the variables and put $\boldsymbol{\theta}$ in the first place in the approximation of q_t . Then the first

part of the preconditioner \mathcal{T}_t is simplified to $\mathcal{T}_t^{(\theta)}(\mathbf{u}_\theta) = \mathcal{S}_{t-1}^{-1} \circ (\mathcal{F}_t^{-1})^{(\theta)}(\mathbf{u}_\theta)$, which avoids the nested preconditioning. The ranks of the auxiliary tensor train can be low for the same reason stated in Remark 5.3. Thus the computational cost is low due to the low dimension d and the low ranks.

Remark 5.5. The map \mathcal{T}_t in (5.9) couples the uniform density and the approximate posterior density of interest. The parameter part $\mathcal{T}_t^{(\theta)}$ is composed of all the previous KR rearrangement \mathcal{F}_k^θ for $k \leq t-1$. But the map for the states is only composed of the KR rearrangement in two steps; for example, the map for \mathbf{u}_{t-1} is given by $\mathcal{T}_{t-1}^{(t-1)} \circ (\mathcal{F}_{t-1}^{-1})^{(t)}$, where $\mathcal{T}_{t-1}^{(t-1)} = (\mathcal{F}_{t-1}^{-1})^{(t-1)}$. This confirms the work in [26, Theorem 12], which presents the decomposition for joint parameter and state estimation in general state space models.

The preconditioner \mathcal{T}_t defined above is not the only non-linear preconditioner suitable for state space models. Potential candidates includes $(\mathcal{L}_t)_\# p_U(\boldsymbol{\theta}, \mathbf{x}_t, \mathbf{x}_{t-1}) = \tilde{p}(\boldsymbol{\theta}, \mathbf{x}_{t-1} | \mathbf{y}_{1:t-1}) f(\mathbf{x}_t | \mathbf{x}_{t-1}, \boldsymbol{\theta})^\alpha g(\mathbf{y}_t | \mathbf{x}_t, \boldsymbol{\theta})^\beta$, for $\alpha, \beta \in (0, 1)$. This is known as a tempering approach and has proved efficient in tempered Kalman filter [15], especially when the data is accurate and thus the likelihood function concentrates on some manifold. However, we can not characterize such \mathcal{L}_t directly from the \mathcal{F}_{t-1} as in (5.7). Instead we need to establish a squared tensor-train approximation of $\tilde{p}(\boldsymbol{\theta}, \mathbf{x}_{t-1} | \mathbf{y}_{1:t-1}) f(\mathbf{x}_t | \mathbf{x}_{t-1}, \boldsymbol{\theta})^\alpha g(\mathbf{y}_t | \mathbf{x}_t, \boldsymbol{\theta})^\beta$ to obtain \mathcal{L}_t , which doubles the computation complexity in each iteration. Such preconditioning is still efficient in complex models with concentrated posteriors. See Section 6 for numerical instances.

Remark 5.6. The uniform reference random variables $\mathbf{V} = \mathbf{U}$ leads to complicated boundaries in the tensor-train approximation of q_t . To avoid it, we can apply standard multivariate Gaussian as reference, i.e., $\mathbf{V} \sim \mathcal{N}(0, I_{2m+d})$. Then the new preconditioner $\bar{\mathcal{L}}_t$ is supposed to map $(\mathbf{v}_\theta, \mathbf{v}_t, \mathbf{v}_{t-1})$ to $(\boldsymbol{\theta}, \mathbf{x}_t, \mathbf{x}_{t-1})$ and thus takes the form $\bar{\mathcal{L}}_t = \mathcal{L}_t \circ \mathcal{R}$, where \mathcal{R} is the lower-triangular KR rearrangement from $\mathcal{N}(0, I_{2m+d})$ to $\text{Uni}([0, 1]^{2m+d})$. The linear preconditioner can also be applied.

6. Numerical results. In this section, we provide several numerical experiments to demonstrate the efficiency of our tensor-train-based method. These includes a state space model with linear state and observation process and Gaussian noise, where the analytical posterior density of the parameters can be derived, a stochastic volatility model with non-linear observation process, a predator and prey model, and a filter problem in Lorenz 96 model. We also contrast our method to the SMC^2 method which is considered as the state-of-the-art particle method for sequential inference for both parameters and states in the literature.

6.1. Kalman Filter. We first consider the SSM with the following linear state and observation process for $\vec{x}_k \in \mathbb{R}^n, \vec{y}_k \in \mathbb{R}^n$,

$$(6.1) \quad \begin{cases} \vec{x}_{k+1} - \mu &= b(\vec{x}_k - \mu) + a\vec{e}_{k+1} \\ \vec{y}_{k+1} &= C\vec{x}_{k+1} + d\vec{e}_{k+1} \end{cases},$$

where \vec{e}_k and \vec{e}_k follow n -dimensional *i.i.d* standard normal distributions. The conditional distribution for the initial state \vec{x}_0 is given by $\vec{x}_0 | \mu, a \sim N(\mu \vec{\mathbf{1}}, a^2 I_n)$. Here $\vec{\mathbf{1}}$ is the n -dimensional vector with all elements to be one, I_n is the n -dimensional identity matrix, μ, a, b, d are scalars. Note that this model is exactly the Kalman filter if the parameters are known. Thus the posterior distribution of the parameters and states can be characterized.

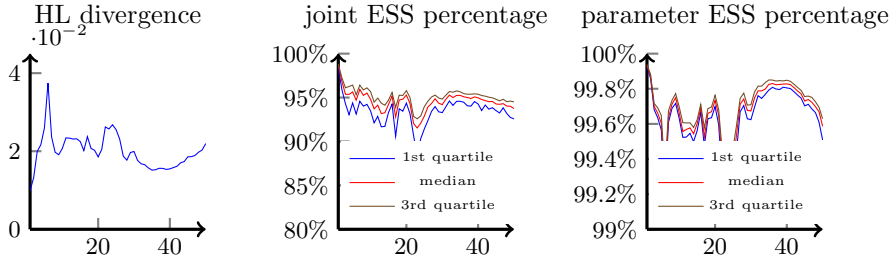


Fig. 1: statistics from FTT-based method; LEFT: the Hellinger divergence between the approximate parameter posterior PDF and its theoretical value. MID: the ESS for samples from joint posterior distribution $p(\theta, x_{0:50}|y_{1:50})$. RIGHT: the ESS for samples from parameter posterior distribution $p(\theta|y_{1:50})$.

In our example, we take the dimension of the states n to be three and the time T to be 50. Then we fix parameter $\mu = 0$. The matrix C is a random matrix filled with i.i.d normal random numbers, which is generated in the initial setup and fixed during the experiment. We enforce the condition $a^2 + b^2 = 1$ so that the states $\{X_k\}$ become a stationary process. This way the parameters to be estimated is $\theta = (a, d)$. We set $a = 0.8$, $d = 0.5$ to generate synthetic data for our experiments. The prior distribution for θ is $U(0.4, 1)$. The posterior distribution $p(\theta|y_{1:T})$ in this case is derived in appendix.

We first present the Hellinger divergence between the approximate parameter posterior density in our tensor-train-based filter and the exact posterior density in 1 (left). The Hellinger divergence remains a low level along time, indicating our method provides good approximation to the parameter posterior density. Figure 1 (mid and right) reports the ESS from tensor-train-based sampler proposed in Section 3, the middle one for all the states together with the parameters, $(\theta, x_{0:T}|y_{1:T})$ and the right one for the parameters only, $(\theta, x_{0:T}|y_{1:T})$. We can see the ESS for the 155-dimensional joint posterior is above 90% after 50 steps. And the ESS for only the parameters is even better, as expected. Thus our method also provides good approximation in the smoothing problem.

Then we compare the tensor-train-based filter with the SMC^2 method. We implement SMC^2 with the particle number of parameters $N_\theta = 500$ and the initial particle number of states $N_x = 100$. These numbers are chosen such that the computing time of tensor-train-based method and SMC^2 are comparable. The kernel density estimation (KDE) method is used to provide an approximation of posterior density based on samples. Figure 2, 3 and 4 present the theoretical parameter posterior density and the approximate parameter posterior PDF from the above two methods at time $T = 10, 30, 50$ respectively. Note the error in SMC^2 method partially come from the KDE approximation. We can see the posterior density from tensor-train-based method appear almost the same as the theoretical one. We conclude our method outperforms the SMC^2 in this example.

6.2. Stochastic Volatility Model. The stochastic volatility model is a non-linear SSM that is widely used in the modelling of financial derivatives. It takes the form

$$\begin{cases} x_{k+1} &= \phi x_k + \sigma \eta_{k+1} \\ y_{k+1} &= \epsilon_{k+1} \beta \exp\left(\frac{x_{k+1}}{2}\right), \end{cases}$$

where ϵ_k and η_k follow i.i.d standard normal distributions and the initial distribution is given as follows, $x_0 \sim N\left(0, \frac{\sigma^2}{1-\phi^2}\right)$. In our example we fix $\sigma = 1$ and use parameters

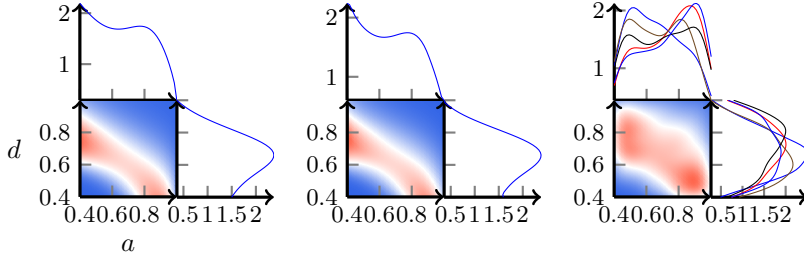


Fig. 2: The joint distribution for (a,d) at time 10, with their marginal distributions on each side. Left: theoretical distribution. Mid: FTT-approximated distribution. Right: SMC^2 estimation with KDE.

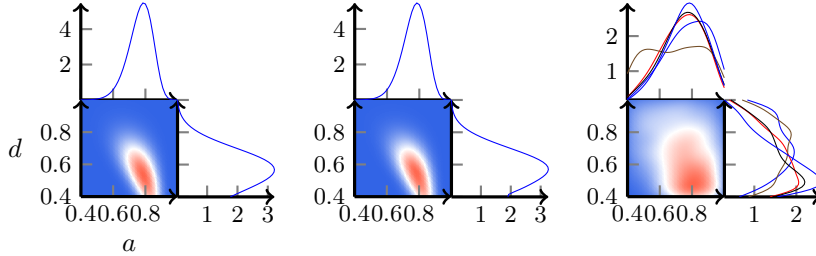


Fig. 3: The joint distribution for (a,d) at time 30, with their marginal distributions on each side. Left: theoretical distribution. Mid: FTT-approximated distribution. Right: SMC^2 estimation with KDE.

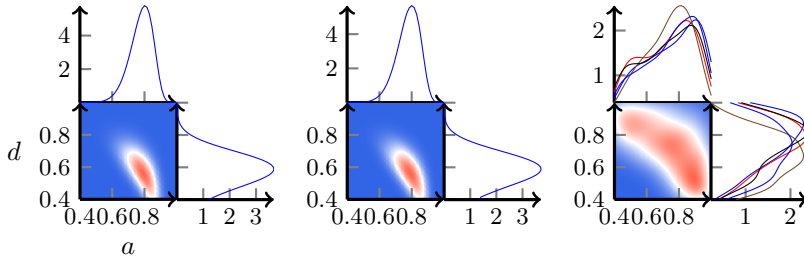


Fig. 4: The joint distribution for (a,d) at time 50, with their marginal distributions on each side. Left: theoretical distribution. Mid: FTT-approximated distribution. Right: SMC^2 estimation with KDE.

$\theta = (\phi, \beta)$. With the true value $\phi = 0.6$ and $\beta = 0.4$ we generate the synthetic states and observations up to $T = 1000$. In this example we can not analytically derive the posterior PDF of θ . Instead, we can compute the joint posterior density for the parameters with all the states $(\phi, \beta, x_{1:1000})$ using ??, so here we use the ESS for the joint posterior density to measure the efficiency.

We present the results with tensor-train ranks 5, 10, and 20 in figure 5. We can see the tensor-train approximation with rank 10 is good enough to provide a reliable result with ESS still over 10% after 1000 steps. Note this is the ESS for the joint posterior density and that for the parameter posterior density is supposed to be better as shown in the Kalman filter example. Then we contrast our method to the SMC^2 with the number of samples $N_\theta = 1000$. Figure 6 provides the posterior PDF of θ at steps 400, 700 and 1000 whereas figure 7 provides the KDE results from five independent runs using SMC^2 method. The posterior from the tensor-train method concentrate around the true parameter values and the high level of ESS indicates this is a reliable result.

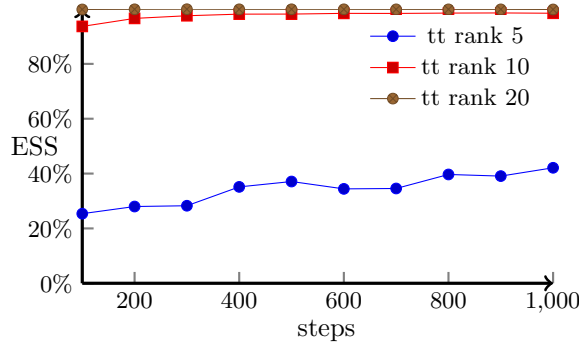


Fig. 5: ESS for joint posterior in stochastic volatility model

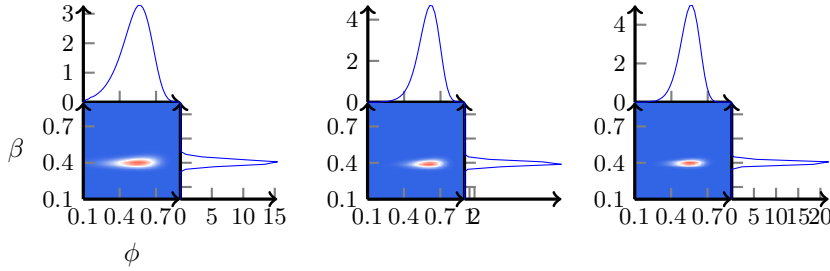


Fig. 6: The joint distribution for (ϕ, β) from FTT approximation with their marginal distributions on each side, at time 400, 700, 1000 individually.

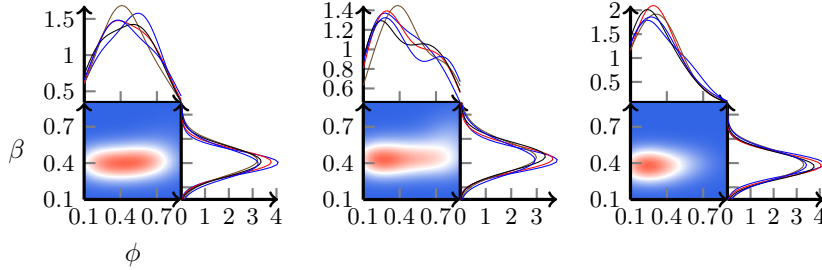


Fig. 7: The joint distribution for (ϕ, β) from SMC^2 estimation with their marginal distributions on each side, at time 400, 700, 1000 individually.

6.3. Predator and Prey Model. The predator and prey model is a challenging model in parameter estimation problem due to the complicated dependency between the parameters. It consists of two first-order non-linear differential equations which describe the dynamics of two species in a biological system, one as a predator and the other as prey 6.2.

$$(6.2) \quad F(P, Q, \theta) := \begin{cases} \frac{dP}{dt} & = rP\left(1 - \frac{P}{K}\right) - s\left(\frac{PQ}{a+P}\right) \\ \frac{dQ}{dt} & = u\left(\frac{PQ}{a+P}\right) - vQ \end{cases}$$

Here P and Q are the sizes of prey and predator with initial condition $P(t=0) = P_0$ and $Q(t=0) = Q_0$ respectively, and $\theta = (r, K, a, s, u, v)$ is the parameter that govern the system. To define the state and parameter estimation problem, we assume the model in 6.2 is perturbed by random noise of discrete time $\epsilon_k \sim N((0, 0)^\top, 25I_2)$ with interval $\Delta t = 4$. For simplicity, we set $P_k = P(t = k\Delta t)$, $Q_k = Q(t = k\Delta t)$ and $X_k = (P_k, Q_k)$, then

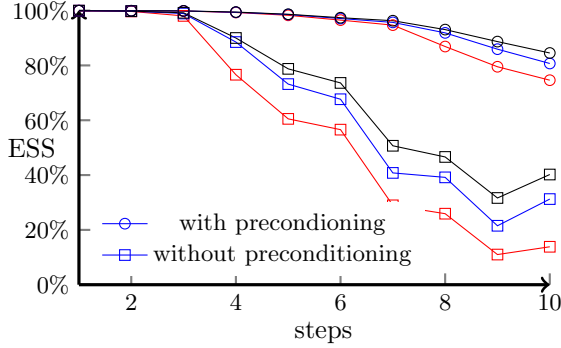


Fig. 8: ESS for joint posterior in predator prey model: red lines are the 1st quantiles, blue lines are the medians, black lines are the 3rd quantiles

$$(6.3) \quad X_{k+1} = X_k + \int_{k\Delta t}^{(k+1)\Delta t} F(P_k, Q_k, \theta) dt + \epsilon_k$$

with initial condition $(P_0, Q_0) = (50, 5)$. We use ode45 solver to evaluate the time integral in 6.3. Then the observations are perturbed by random noise $\vec{\eta}_k \sim N(0, I_2)$,

$$Y_{k+1} = X_{k+1} + \eta_k.$$

We use $\theta = (0.6, 100, 30, 1.2, 0.5, 0.3)$ to generate synthetic data up to 20 steps, shown in figure 8.

The figure presents the joint ESS of the parameters and all the states along time. We first notice the plain tensor-train method decreases rapidly in the first 10 steps, due to the complicated dependency between parameters. Rather than violently increase the rank of tensor trains to enhance its approximation power, we apply the preconditioning method as detailed in section 4. We observe the ESS in the preconditioning method is increased efficiently in the first 10 steps.

Thus the tensor-train method with preconditioning is capable to work on the model with complicated dependency between parameters.

6.4. Lorenz 96 Model. The Lorenz 96 model is a system of three coupled ordinary differential equations in the form of,

$$(6.4) \quad \frac{d\vec{x}_t}{dt} = F(\vec{x}_t, \theta),$$

with some initial condition and θ to be the parameters that govern the system. The function $F = [F_1, F_2, \dots, F_n]$, $n \geq 4$ takes the form,

$$(6.5) \quad F_i(\vec{x}_t) = (x_{t,i+1} - x_{t,i-2})x_{t,i-1} - x_{t,i} + C.$$

Here C is a forcing constant and $x_{t,i}$ is the i -th dimension of the state at time t , with $x_{t,-1} = x_{n-1}$, $x_0 = x_n$, and $x_{n+1} = x_1$ as convention. The constant C is a forcing term and we take $C = 8$, which causes chaotic behaviour of the system.

The system is notable for having chaotic solutions for certain parameter values and initial conditions, i.e., the trajectory will appear quite differently using different parameters. To define the state and parameter estimation problem, we assume the model in 6.4 is perturbed by random noise of discrete time $\vec{\epsilon}_k \sim N(0, 0.1 \times I_8)$ with

interval $\Delta t = 0.1$. As in predator and prey model, we set $\vec{x}_k = \vec{x}_{k\Delta t}$,

$$(6.6) \quad \vec{x}_{k+1} = \int_{k\Delta t}^{(k+1)\Delta t} F(\vec{x}_t) dt + \vec{x}_k + \vec{\epsilon}_k,$$

with initial condition $x_{0,i} = 1$ for $i = 1, 2, \dots, n$. As before, we use ode45 solver to evaluate the time integral in 6.6. Then the states are corrupted by some observations with i.i.d observation error $\vec{\eta}_k \sim N(0, 0.1 \times I_8)$,

$$(6.7) \quad \vec{y}_k = \vec{x}_k + \vec{\eta}_k.$$

We take $n = 5$ and $C = 8$, which causes chaotic behaviour of the system and only perform state estimation using tensor-train format in such a chaotic model. Fig 9 shows the ESS for the joint posterior for all the states and parameters up to step 50. It is notable that our method remains efficient with ESS to be 20% for a 250-dimensional state estimation problem.

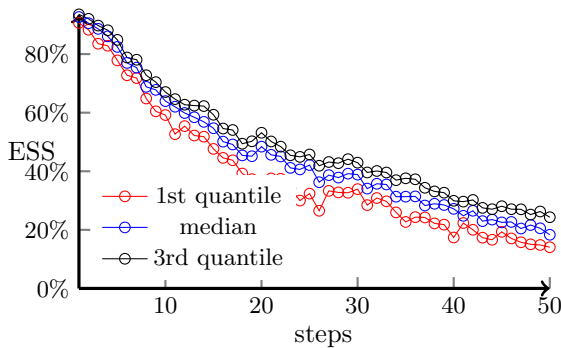


Fig. 9: ESS for joint posterior in Lorenz96 model

7. Conclusion. We propose a novel tensor-train-based method to solve the inference problem of both states and parameters in state space models. The main result of our method is the direct approximation of the posterior density rather than the particle representation. The computational cost is linear in time. Thus we prevent the problem of both the particle degeneration and the curse of dimensionality.

The limitation of our method comes from the accuracy of the function approximation. The preconditioning technique to improve the accuracy is discussed but yet there is no proved result for reducing the tensor-train ranks. Hence some known structure with lower tensor-train rank is of interest, such as the conditional Gaussian model. The ongoing work includes the method to reduce tensor-train ranks and the exploration in low-rank structure.

Appendix A. f -divergence of marginal random variables. Commonly used statistical divergences such as Kullback–Leibler divergence, total variation distance and squared Hellinger distance are all instances of the f -divergence. Given a convex function $f(\cdot)$, the f -divergence takes the form

$$D_f(p||q) = \int f\left(\frac{p(\mathbf{x})}{q(\mathbf{x})}\right)q(\mathbf{x})d\mathbf{x},$$

The following lemma bounds the f -divergence of marginal random variables by the corresponding f -divergence of joint random variables.

LEMMA A.1. Let $p(\mathbf{x}_1, \mathbf{x}_2)$ and $q(\mathbf{x}_1, \mathbf{x}_2)$ be two joint densities and $\bar{p}(\mathbf{x}_1)$ and $\bar{q}(\mathbf{x}_1)$ are the marginal densities of p and q , respectively. Then the f -divergence of $\bar{p}(\mathbf{x}_1)$ from $\bar{q}(\mathbf{x}_1)$ is bounded from above by that of $p(\mathbf{x}_1, \mathbf{x}_2)$ from $q(\mathbf{x}_1, \mathbf{x}_2)$, i.e.,

$$D_f(\bar{p}||\bar{q}) \leq D_f(p||q).$$

Proof. Since the function f is convex, applying Jensen's inequality, we have

$$\begin{aligned} D_f(p||q) &= \mathbb{E}_{q(\mathbf{x}_1, \mathbf{x}_2)} \left[f \left(\frac{p(\mathbf{X}_1, \mathbf{X}_2)}{q(\mathbf{X}_1, \mathbf{X}_2)} \right) \right] \\ &= \int \int \left(f \left(\frac{p(\mathbf{x}_1, \mathbf{x}_2)}{q(\mathbf{x}_1, \mathbf{x}_2)} \right) \frac{q(\mathbf{x}_1, \mathbf{x}_2)}{\bar{q}(\mathbf{x}_1)} d\mathbf{x}_2 \right) \bar{q}(\mathbf{x}_1) d\mathbf{x}_1 \\ &\geq \int f \left(\int \frac{p(\mathbf{x}_1, \mathbf{x}_2)}{q(\mathbf{x}_1, \mathbf{x}_2)} \frac{q(\mathbf{x}_1, \mathbf{x}_2)}{\bar{q}(\mathbf{x}_1)} d\mathbf{x}_2 \right) \bar{q}(\mathbf{x}_1) d\mathbf{x}_1 \\ &= \int f \left(\int \frac{p(\mathbf{x}_1, \mathbf{x}_2)}{\bar{q}(\mathbf{x}_1)} d\mathbf{x}_2 \right) \bar{q}(\mathbf{x}_1) d\mathbf{x}_1 \\ &= \int f \left(\frac{\bar{p}(\mathbf{x}_1)}{\bar{q}(\mathbf{x}_1)} \right) \bar{q}(\mathbf{x}_1) d\mathbf{x}_1 = D_f(\bar{p}||\bar{q}), \end{aligned}$$

which concludes the proof. \square

When the densities are only known up to some constants, the L^2 distance between the square root of the unnormalized marginal densities is also bounded by that of the unnormalized joint densities. This is shown in the following lemma.

LEMMA A.2. Let $\pi_1(\mathbf{x}_1, \mathbf{x}_2)$ and $\pi_2(\mathbf{x}_1, \mathbf{x}_2)$ be two unnormalized joint densities and $\bar{\pi}_1(\mathbf{x}_1) = \int \pi_1(\mathbf{x}_1, \mathbf{x}_2) d\mathbf{x}_2$ and $\bar{\pi}_2(\mathbf{x}_1) = \int \pi_2(\mathbf{x}_1, \mathbf{x}_2) d\mathbf{x}_2$ are their corresponding unnormalized marginal densities. Then the L^2 distance between $\sqrt{\bar{\pi}_1}(\mathbf{x}_1)$ and $\sqrt{\bar{\pi}_2}(\mathbf{x}_1)$ is bounded from above by the L^2 distance between $\sqrt{\pi_1(\mathbf{x}_1, \mathbf{x}_2)}$ and $\sqrt{\pi_2(\mathbf{x}_1, \mathbf{x}_2)}$, i.e.,

$$\|\sqrt{\bar{\pi}_1} - \sqrt{\bar{\pi}_2}\|_{L^2} \leq \|\sqrt{\pi_1} - \sqrt{\pi_2}\|_{L^2}.$$

Proof. The L^2 distance between $\sqrt{\pi_1}$ and $\sqrt{\pi_2}$ can be expressed as

$$\begin{aligned} \|\sqrt{\pi_1} - \sqrt{\pi_2}\|_{L^2}^2 &= \int \int (\sqrt{\pi_1(\mathbf{x}_1, \mathbf{x}_2)} - \sqrt{\pi_2(\mathbf{x}_1, \mathbf{x}_2)})^2 d\mathbf{x}_1 d\mathbf{x}_2 \\ &= \int \int \left(\sqrt{\frac{\pi_1(\mathbf{x}_1, \mathbf{x}_2)}{\pi_2(\mathbf{x}_1, \mathbf{x}_2)}} - 1 \right)^2 \pi_2(\mathbf{x}_1, \mathbf{x}_2) d\mathbf{x}_1 d\mathbf{x}_2 \\ &= \int \int \left(\sqrt{\frac{\pi_1(\mathbf{x}_1, \mathbf{x}_2)}{\pi_2(\mathbf{x}_1, \mathbf{x}_2)}} - 1 \right)^2 \frac{\pi_2(\mathbf{x}_1, \mathbf{x}_2)}{\bar{\pi}_2(\mathbf{x}_1)} d\mathbf{x}_2 \bar{\pi}_2(\mathbf{x}_1) d\mathbf{x}_1. \end{aligned}$$

Since $f(r) = (\sqrt{r} - 1)^2, r \geq 0$ is a convex function. Applying Jensen's inequality to the inner integral over $d\mathbf{x}_2$, the rest of the proof follows the same steps of A.1. \square

REFERENCES

- [1] C. ANDRIEU, A. DOUCET, AND R. HOLENSTEIN, *Particle markov chain monte carlo methods*, Journal of the Royal Statistical Society: Series B (Statistical Methodology), 72 (2010), pp. 269–342.
- [2] D. BIGONI, A. P. ENGSIG-KARUP, AND Y. M. MARZOUK, *Spectral tensor-train decomposition*, SIAM Journal on Scientific Computing, 38 (2016), pp. A2405–A2439.

- [3] V. I. BOGACHEV, A. V. KOLESNIKOV, AND K. V. MEDVEDEV, *Triangular transformations of measures*, Sbornik: Mathematics, 196 (2005), pp. 309–335.
- [4] O. CAPPÉ, E. MOULINES, AND T. RYDÉN, *Inference in Hidden Markov Models*, Springer Science & Business Media, 2006.
- [5] N. CHOPIN, P. E. JACOB, AND O. PAPANASTASIIOPOULOS, *Smc2: an efficient algorithm for sequential analysis of state space models*, Journal of the Royal Statistical Society: Series B (Statistical Methodology), 75 (2013), pp. 397–426.
- [6] T. CUI AND S. DOLGOV, *Deep composition of tensor-trains using squared inverse rosenblatt transports*, Foundations of Computational Mathematics, (2021), pp. 1–60.
- [7] S. V. DOLGOV AND D. V. SAVOSTYANOV, *Alternating minimal energy methods for linear systems in higher dimensions*, SIAM Journal on Scientific Computing, 36 (2014), pp. A2248–A2271.
- [8] A. DOUCET, N. D. FREITAS, AND N. GORDON, *An introduction to sequential monte carlo methods*, in Sequential Monte Carlo methods in practice, Springer, 2001, pp. 3–14.
- [9] A. DOUCET AND A. M. JOHANSEN, *A tutorial on particle filtering and smoothing: Fifteen years later*, Handbook of nonlinear filtering, 12 (2009), p. 3.
- [10] N. J. GORDON, D. J. SALMOND, AND A. F. SMITH, *Novel approach to nonlinear/non-gaussian bayesian state estimation*, in IEE proceedings F (radar and signal processing), vol. 140, IET, 1993, pp. 107–113.
- [11] A. GORODETSKY, S. KARAMAN, AND Y. M. MARZOUK, *A continuous analogue of the tensor-train decomposition*, Computer Methods in Applied Mechanics and Engineering, 347 (2019), pp. 59–84.
- [12] A. A. GORODETSKY, S. KARAMAN, AND Y. M. MARZOUK, *Function-train: A continuous analogue of the tensor-train decomposition*, arXiv preprint arXiv:1510.09088, (2015).
- [13] M. GRIEBEL AND H. HARBRECHT, *Analysis of tensor approximation schemes for continuous functions*, Foundations of Computational Mathematics, (2021), pp. 1–22.
- [14] W. HACKBUSCH, *Tensor spaces and numerical tensor calculus*, vol. 42, Springer Science & Business Media, 2012.
- [15] E. HERBST AND F. SCHORFHEIDE, *Tempered particle filtering*, Journal of Econometrics, 210 (2019), pp. 26–44.
- [16] N. KANTAS, A. DOUCET, S. S. SINGH, AND J. M. MACIEJOWSKI, *An overview of sequential monte carlo methods for parameter estimation in general state-space models*, IFAC Proceedings Volumes, 42 (2009), pp. 774–785.
- [17] H. KNOTHE ET AL., *Contributions to the theory of convex bodies.*, The Michigan Mathematical Journal, 4 (1957), pp. 39–52.
- [18] J. S. LIU, R. CHEN, AND T. LOGVINENKO, *A theoretical framework for sequential importance sampling with resampling*, in Sequential Monte Carlo methods in practice, Springer, 2001, pp. 225–246.
- [19] S. MASKELL AND N. GORDON, *A tutorial on particle filters for on-line nonlinear/non-gaussian bayesian tracking*, IEE Target Tracking: Algorithms and Applications (Ref. No. 2001/174), (2002), pp. 2–1.
- [20] I. OSELEDETS AND E. TYRTYSHNIKOV, *Tt-cross approximation for multidimensional arrays*, Linear Algebra and its Applications, 432 (2010), pp. 70–88.
- [21] I. V. OSELEDETS, *Tensor-train decomposition*, SIAM Journal on Scientific Computing, 33 (2011), pp. 2295–2317.
- [22] M. K. PITT AND N. SHEPHARD, *Filtering via simulation: Auxiliary particle filters*, Journal of the American statistical association, 94 (1999), pp. 590–599.
- [23] S. REICH AND C. COTTER, *Probabilistic forecasting and Bayesian data assimilation*, Cambridge University Press, 2015.
- [24] P. B. ROHRBACH, S. DOLGOV, L. GRASEDYCK, AND R. SCHEICHL, *Rank bounds for approximating gaussian densities in the tensor-train format*, SIAM/ASA Journal on Uncertainty Quantification, 10 (2022), pp. 1191–1224.
- [25] M. ROSENBLATT, *Remarks on a multivariate transformation*, The annals of mathematical statistics, 23 (1952), pp. 470–472.
- [26] A. SPANTINI, D. BIGONI, AND Y. MARZOUK, *Inference via low-dimensional couplings*, The Journal of Machine Learning Research, 19 (2018), pp. 2639–2709.